Inelastic J/ψ-Photoproduction at HERA and the Color Evaporation Model

Diplomarbeit

vorgelegt von

Jan Schümann

II. Institut für Experimentalphysik
Universität Hamburg

Gutachter der Diplomarbeit: Prof. Dr. B. Naroska
Prof. Dr. V. Blobel

Abgabedatum der Diplomarbeit: 28.04.2000

Abstract

An investigation of the color evaporation model is presented. The color evaporation model describes the production of J/ψ mesons. The numerical FMNR program is used to calculate the next to leading order J/ψ production cross sections as predicted by the color evaporation model. Cross sections are calculated as functions of p_T^2, $W_{\gamma p}$ and z. In addition the p_T^2 distribution was investigated in four different z regions. The color evaporation model predictions with and without a phenomenological correction factor introduced by Halzen et al. are investigated. Both are compared with a color singlet model Monte-Carlo generator and with data collected at the HERA collider.

It is found that the data for the p_T^2, $W_{\gamma p}$ and z distributions are in a good agreement with the color evaporation model predictions with the correction factor. The shapes of the double differential p_T^2 distributions for the data however are not described by the corrected distributions of the color evaporation model. For the double differential distributions the predictions without the correction factor are in very good agreement with the data.

Kurzzusammenfassung

In dieser Analyse wurde das Color-Evaporation Modell untersucht. Das Color-Evaporation Modell beschreibt die J/ψ-Meson Produktion. Das numerische FMNR Programm wurde benutzt um die J/ψ Wirkungsquerschnitte des Color-Evaporation Modells in nächst führender Ordnung zu berechnen. Die Wirkungsquerschnitte wurden als Funktion von p_T^2, $W_{\gamma p}$ und z berechnet. Ausserdem wurde die p_T^2 Verteilung in vier unterschiedlichen z Bereichen untersucht. Das Color-Evaporation Modell wurde mit und ohne einem phänomenologischen Korrekturfaktor, der von Halzen et al. eingeführt wurde, untersucht. Beides wurde mit den Prognosen eines Monte-Carlo Generators des Color-Singlet Modells und mit HERA Daten verglichen.

Es wurde festgestellt, dass die Daten von den Verteilungen des korrigierten Color-Evaporation Modells beschrieben werden. Die Form der doppelt differenziellen p_T^2 Verteilungen der Daten kann nicht mit den Verteilungen des Color-Evaporation Modells mit Korrekturfaktor beschrieben werden. Sie wird jedoch von den unkorrigierten Color-Evaporation Modell Verteilungen sehr gut beschrieben.

Contents

Introduction **1**

1 The Experiment H1 **3**

1.1 The HERA Collider 3

1.2 The H1 Detector 4

2 Kinematics and Models of J/ψ Production **6**

2.1 HERA Kinematics 6

2.1.1 ep Kinematics at H1 6

2.1.2 J/ψ Kinematics 8

2.2 J/ψ Production Mechanisms 9

2.2.1 Pointlike J/ψ -Production (Boson-Gluon Fusion) 9

2.2.2 Hadronic J/ψ-Production 11

2.3 Models for J/ψ Production 11

2.3.1 The Color Singlet Model 12

2.3.2 NRQCD or the Color Octet Model 13

2.3.3 The Color Evaporation Model 13

2.4 Comparison with Experimental Data 19

3 Monte-Carlo Generators and Theory Programs **22**

3.1 Monte-Carlo Generators 22

3.1.1 EPJPSI: Color Singlet Monte-Carlo Generator 22

3.1.2 RAPGAP: Monte-Carlo Generator for Heavy Quark Production 23

3.2 FMNR: Next to Leading Order Program for Heavy Quark Production 23

4 Results **26**

4.1 The FMNR program 26

4.1.1 Validating the FMNR program 27

4.1.2 Calculation of the Color Evaporation Model 27

4.1.3 The Effects of Kinematical Cuts 30

4.2 Comparison of the FMNR Predictions with other Calculations 31

4.2.1 Comparison of Leading and Next to Leading Order Predictions of RAPGAP and the FMNR Program 34

4.2.2 Comparison of the Predictions of the FMNR Program and Halzen et al. 36

4.2.3 Comparison of EPJPSI and the FMNR Predictions 37

4.2.4 Comparison of the Berger-Jones Cross Section and the Cross Section of the FMNR Program 40

4.3 Comparison of the FMNR predictions with Data 40

4.3.1 Comparison of Differential Cross Sections 41

4.3.2 Comparison of Double Differential Distributions 43

4.4 Conclusions from the Comparisons 47

Summary **48**

A The Complete Settings **56**

A.1 For EPJPSI 56

A.2 For RAPGAP 56

A.3 For the FMNR program 56

A.3.1 For the Pointlike Component of the FMNR program 56

A.3.2 For the Hadronic Component of the FMNR program 57

A.4 Scaling Factors 57

List of Figures **61**

List of Tables **63**

Bibliography **64**

Introduction

Starting in 1992 electron-proton collisions are investigated at DESY (Deutsches Elektronen Synchrotron) in Hamburg. This unique accelerator is operating at a center of mass energy of $\sqrt{s} = 300\,\mathrm{GeV}$. This is approximately one order of magnitude higher than any fixed target experiment, making a wide region of physics accessible, such as measurements of the proton structure function, measurements of the parton distribution of photons, tests of perturbative QCD and the quest for new particles.
The goal of high energy particle physics is the understanding of the fundamental interactions between the elementary constituents of matter. The *standard model* provides a satisfactory framework for particle physics. Over the past 20 years only very few statistically irrelevant deviations from the standard model were observed.
The beginning of heavy quark physics is marked by the discovery of the J/ψ meson in 1974. The J/ψ meson is a bound $c\bar{c}$ pair. Three years later the Υ meson consisting of a bound $b\bar{b}$ pair was observed. Surprisingly the description of the high production rates for J/ψ mesons at the TEVATRON is a major challenge for the standard model. The production rates predicted by the color singlet model are more than one order of magnitude below TEVATRON data. New parameters, the color octet matrix elements, were introduced which are expected to be universal. The matrix elements for the color octet model were extracted from the TEVATRON data. Therefore the color octet model can describe the high production rates at the TEVATRON correctly. The color octet model however does not give a satisfactory description of the HERA data.
In the present analysis a third model to describe J/ψ meson production is investigated, the color evaporation model. In the color evaporation model the color of the produced $c\bar{c}$ pair is assumed to be 'bleached out' (evaporate) by multiple soft gluon interactions. This implies a statistical treatment of color. The cross section for J/ψ production in the color evaporation model is calculated by integrating the $c\bar{c}$ cross section over a mass interval of $[2m_c, 2m_D]$. In order to obtain the statistical rate for the production of the color singlet state of the J/ψ meson, a factor of $\frac{1}{9}$ is applied to the cross section. In addition a factor $\rho_{J/\psi}$ is multiplied to the cross section. This factor represents the fraction of color singlet $c\bar{c}$ pairs that evolve into a J/ψ meson.
In this thesis the cross sections for J/ψ production in the color evaporation model are calculated using the FMNR program. It is a program to calculate open $c\bar{c}$ pair production in next to leading order. J/ψ production in the color singlet model and the color evaporation model are compared for photoproduction events in ep collisions. In addition the cross sections are compared to the data taken at HERA from 1995 to 1997. The data selection is described in detail in [Kru00].
In **chapter 1** a short overview of the HERA collider and the H1 detector with its major components is given. ep kinematics and the kinematics of J/ψ meson production are described

in the first part of **chapter 2**. In the second part the production processes of J/ψ mesons are introduced. In the third part the three major models to describe J/ψ production are presented. The Monte-Carlo generators EPJPSI and RAPGAP and the FMNR program used in this analysis are described in **chapter3**. In **chapter 4** the implementation of the color evaporation model is explained and comparisons with Monte-Carlo generators are made. In addition the color evaporation model predictions are compared with the data.

Chapter 1

The Experiment H1

HERA (**H**adron-**E**lektron-**R**ing-**An**lage) is a unique storage ring system at DESY (**D**eutsches **E**lektron **Sy**nchrotron) in Hamburg, Germany. It was built in 1990 after six years of construction. This project allows to accelerate, store and collide protons and electrons[1] in two counter rotating beams at a center of mass energy of 300 GeV. The first ep collisions at HERA were observed in 1991 and since 1992 the two multi-purpose detectors H1 and ZEUS are taking data. In this chapter a short overview of the collider and the H1 experiment is given.

1.1 The HERA Collider

The world's first electron-proton collider HERA was built with two independent storage rings of 6.4 km circumference. The electrons and protons are passing several preaccelerators before entering the HERA storage ring (see fig. 1.1).

The electrons are stored at an energy of 27.5 GeV and the protons are stored at 820 GeV resulting in a center of mass energy of $\sqrt{s} \approx 300\,\text{GeV}$.[2] When colliding head-on the two beams have nearly zero crossing angle at the two interaction points in the north and the south, at the H1 and ZEUS detector, respectively. In 1995 the HERMES detector was added. It used only the polarized electron beam to investigate the spin nature of nucleons in a fixed gas-target. Since 1998 HERA-B is using the proton beam to look for CP-violation in the system of B-mesons.
The electrons and protons are stored in up to 220 bunches, resulting in a time distance between two bunchcrossings of 96 ns or a frequency of 10.4 MHz. The average beam lifetime is typically 10 hours, which is dominated by the electron lifetime ($\approx 10\,\text{h}$) not by the proton lifetime ($\approx 24\,\text{h}$). For the study of background conditions some bunches have no collision partner (pilot bunches). Background originates from interactions of the beams with rest gas molecules in the beampipe, with the beampipe itself, or from synchrotron radiation or cosmics.

[1] At HERA it is possible to use either electrons or positrons for the electron beam. From 1994 to 1997 positrons were used instead of electrons to increase the lifespan of the beam. Furthermore the word electrons stands for positrons as well.

[2] HERA is operating with a 920 GeV proton beam since 1998. Since the data used in this analysis were taken before 1998 the beam energy will be taken to be 820 GeV.

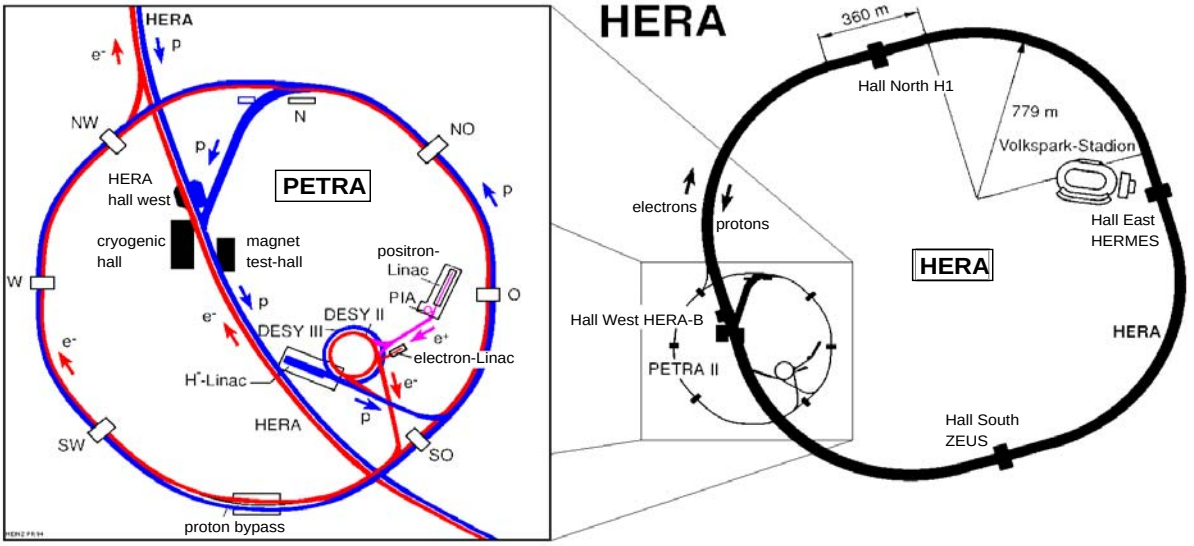

Figure 1.1: The storage ring HERA (right) and its preaccelerators (left) at DESY.

1.2 The H1 Detector

The H1 detector was built according to the same principles of most modern collider experiments. Due to the different beam energies of HERA the *ep* system is strongly boosted along the proton direction. The asymmetric layout of the H1 detector takes this into account. In the direction of the proton beam there is a more massive instrumentation. A detailed description of the H1 detector can be found in [H1]. The H1 detector is a multi purpose detector demanding high resolutions for a large number of variables. For example excellent electron identification and measurement is required in order to study deep inelastic scattering and physics precise momentum measurements and good muon identification are necessary for heavy flavor physics. This hardware setup has to be combined with an efficient software to guarantee efficient and accurate data taking. A schematic overview of the H1 detector is given in figure 1.2. The beam pipe 1 [3] is surrounded by the tracking system, consisting of the central tracker 2, the forward tracker 3 and the central silicon tracker (not indicated in the figure). The electromagnetic 4 and the hadronic 5 liquid argon calorimeter are embedded in the cryostat 15 which cools a superconducting coil. The tracking system and the calorimeter are surrounded by a superconducting solenoid 6, producing a magnetic field parallel to the beam pipe of 1.6 T. The instrumented iron 10 and the muon toroid magnet 11 form the outer layers of the detector. The origin of the coordinate system for H1 physics is the interaction point of the two beams, as marked with a small cross in the beampipe in figure 1.2. The *z*-axis is along the proton beam, the *x*-axis points to the center of the HERA ring and the *y*-axis is according to a right-handed coordinate system. The coordinate system is conventionally described in spheric coordinates with the angles θ and ϕ. θ is the angle between the *z* axis and the particle track, ϕ describes direction of the track.

[3] The numbers correspond to the numbers in fig. 1.2

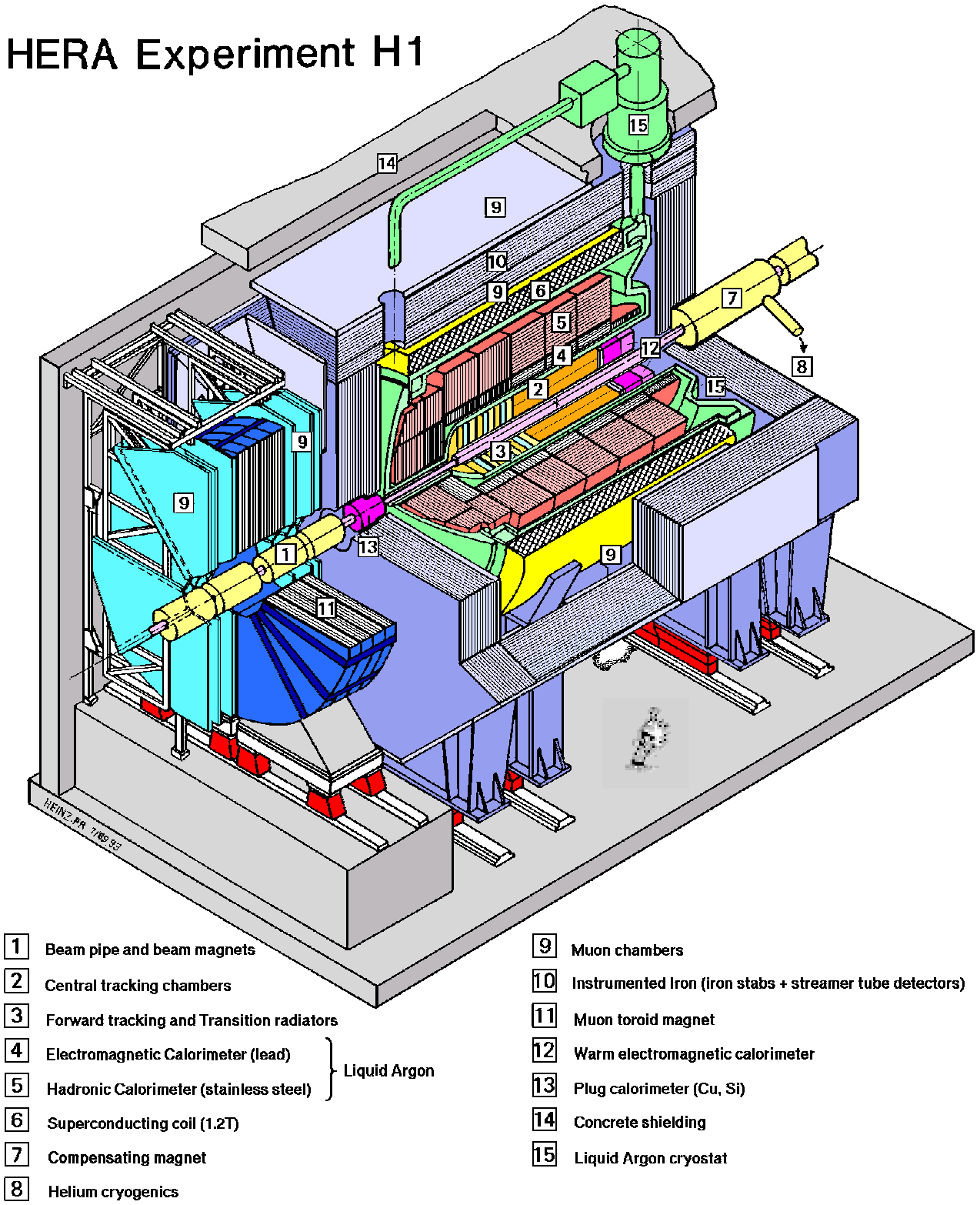

Figure 1.2: A schematic overview of the H1 detector.

Chapter 2

Kinematics and Models of J/ψ Production

In this chapter the HERA kinematics are introduced and the production processes of J/ψ mesons are described.
Subsequently the three main models to describe inelastic J/ψ photoproduction are presented.

2.1 HERA Kinematics

In this section HERA kinematics for J/ψ production are discussed. At first the general ep kinematics are introduced, followed by a more detailed view on J/ψ production kinematics.

2.1.1 ep Kinematics at H1

At the HERA collider electrons and protons are accelerated to beam energies of $E_e = 27.5\,\text{GeV}$ and $E_p = 820\,\text{GeV}$ respectively. Conveniently Lorentz invariant quantities are used for the description of the kinematics. The squared center of mass energy s of the collision is given by:

$$s = (k+p)^2 \approx 4E_eE_p \approx (300\,\text{GeV})^2, \tag{2.1}$$

where k and p are the four momenta of the incoming electron and proton respectively. Here and in the following the masses are neglected for the approximation.
The basic process for deep inelastic scattering in ep collisions is illustrated in figure 2.1. Electron proton scattering is in lowest order described by the exchange of a single gauge boson. In neutral current (NC) events a photon or a Z^0-boson is exchanged, in charged current (CC) events a $W^{\pm}$-boson. Due to the heavy mass of the weak bosons W and Z^0, $m_W \approx 80\,\text{GeV}$, $m_W \approx 91\,\text{GeV}$, electron proton scattering via the W or Z^0 boson exchange is suppressed for $Q^2 \ll m_W^2$.
Events can be classified by the *virtuality* of the photon Q^2,

$$Q^2 = -q^2 = -(k-k')^2, \tag{2.2}$$

with q and k' being the four momenta of the photon and the outgoing electron respectively (see figure 2.1). At HERA events are separated into two kinematical regions:

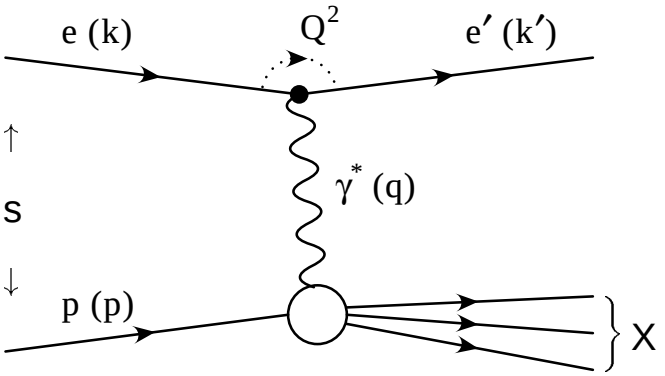

Figure 2.1: A generic diagram for ep scattering. X designates any hadronic final state, the variables are described in the text.

- **Photoproduction:** $Q^2 \approx 0$. In this Q^2 range the electron is scattered under very small angles and cannot be detected in the central detector region. It may be detected by a special small angle electron detector.
- **Deep inelastic scattering:** $Q^2 \geq m_p^2$, m_p being the proton rest mass. Under this condition the scattered electron is detected in the central detector.

For Photoproduction the photon-proton center of mass energy $W_{\gamma p}$ and the Lorentz invariant s are related as:

$$W_{\gamma p}^2 = (p+q)^2 \approx y \cdot s, \tag{2.3}$$

where the *inelasticity y* is the Lorentz invariant scaling variable defined as:

$$y = \frac{q \cdot p}{k \cdot p} \approx \frac{E_e - E_e'}{E_e}. \tag{2.4}$$

Here E_e' is the energy of the scattered electron. In the proton rest frame y is the fractional energy loss of the scattered electron. For equations 2.3 and 2.4 the approximations are again neglecting the masses.
At the high HERA energies a parton, a constituent of the proton, i.e. a quark or a gluon, interacts directly or via another quark with the photon. The Bjorken scaling variable x is defined as:

$$x = \frac{-q^2}{2q \cdot p}. \tag{2.5}$$

It is the fraction of the proton momentum carried by the parton for the pointlike component in the quark parton model. For deep inelastic scattering in the leading order quark parton model it can be identified as the four-momentum of the struck quark in the proton.

Neglecting the masses of the electron and proton we find x, y and Q^2 related by the simple equation:

$$Q^2 \approx xys. \tag{2.6}$$

For photoproduction the radiation of a photon and the interaction with the proton can be treated independently (Weiszäcker Williams approximation [WW]). This allows to factorize the ep cross section:

$$\frac{\mathrm{d}^2\sigma_{ep}(y,Q^2)}{\mathrm{d}y\,\mathrm{d}Q^2} = f_{\gamma/e}(y,Q^2)\sigma_{\gamma p}(y,Q^2), \tag{2.7}$$

with $f_{\gamma/e}$ describing the photonflux and $\sigma_{\gamma p}$ being the photon-proton cross section. In the Weiszäcker Williams approximation $f_{\gamma/e}$ is calculated in [FMNR2] to be:

$$f_{\gamma/e} = \frac{\alpha_{em}}{2\pi}\cdot\frac{(1+(1-y)^2)}{y}\cdot log(\frac{Q^2_{max}}{Q^2_{min}}) + \frac{\alpha_{em}}{2\pi}2m_e^2y(\frac{1}{Q^2_{max}} - \frac{1}{Q^2_{min}}). \tag{2.8}$$

m_e is the electron rest mass, $Q^2_{min} = \frac{(m_e y)^2}{(1-y)}$ is the minimal Q^2 exchanged and Q^2_{max} is the maximum Q^2. $Q^2_{max} = 1\,\mathrm{GeV}$ in this analysis in order to limit the analysis to photoproduction.

2.1.2 J/ψ Kinematics

In 1974 two groups discovered the J/ψ meson simultaneously. Aubert et al. [Aub] observed an enhancement in the e^+e^- invariant mass spectrum in Brookhaven, giving evidence of a new particle. They named it J. Augustin et al. [Aug] measured the e^+e^- annihilation cross section at the SPEAR machine in Stanford (SLAC), calling the new particle ψ.
The J/ψ meson is interpreted as a bound state of $c\overline{c}$ quarks with the quantum numbers $J^{PC} = 1^{--}$ and mass $m_{J/\psi} = 3.097\,\mathrm{GeV}$. It is the lightest charmed vector meson in the *Charmonium* family. This is one reason for a special property of the J/ψ meson, the extremely small decay width $\Gamma_{J/\psi} = 87 \pm 5\,\mathrm{keV}$. In addition it has only few options to decay via the strong force. The possible decays are forbidden by the OZI rule [1], leaving the contributions of electromagnetic decays substantial. Lepton universality implies almost identical branching ratios for the decay into e^+e^- and $\mu^+\mu^-$, $BR(J/\psi \to e^+e^-) = (6.02 \pm 0.19)\%$ and $BR(J/\psi \to \mu^+\mu^-) = (6.01 \pm 0.19)\%$.
The transverse momentum p_T of the J/ψ meson is an experimentally important variable to describe J/ψ production. Although the incoming electron and proton do not have a transverse momentum, the interacting partons may have transverse momenta (see figure 2.2) passing them to the produced J/ψ meson. p_T is defined as:

$$p_T = \sqrt{p_x^2 + p_y^2}, \tag{2.9}$$

with p_x and p_y being the x and y component of the J/ψ momentum. The fraction of en-

[1] The OZI rule states that diagrams containing disconnected quark lines are suppressed relative to those with connected ones.

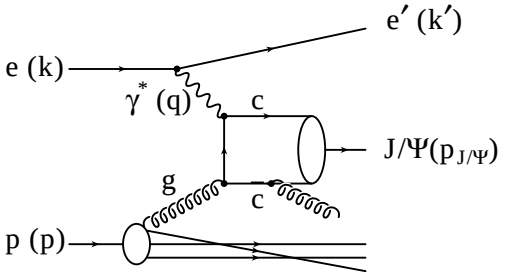

Figure 2.2: J/ψ-production via boson gluon fusion in the color singlet model.

ergy transferred from the photon to the J/ψ meson in the proton rest frame is the *elasticity* z. This Lorentz invariant variable is used to discriminate different production mechanisms and is defined as:

$$z := \frac{p_{J/\psi} \cdot p}{q \cdot p} \approx \frac{E_{J/\psi}}{E_\gamma}, \tag{2.10}$$

where $p_{J/\psi}$ denotes the four momenta of the J/ψ.

2.2 J/ψ Production Mechanisms

2.2.1 Pointlike J/ψ -Production (Boson-Gluon Fusion)

Boson-gluon fusion is the leading order process for quark antiquark pair production illustrated in figure 2.3. The gluon from the proton and the virtual photon from the electron interact via a virtual quark line. This process is sometimes referred to as pointlike (or direct) production. At HERA energies light (u,d,s) and heavy (c,b) quark-antiquark pairs can be produced. The generation of b quarks is suppressed due to the higher energies needed because of the large b quark mass by approximately two orders of magnitude compared to the formation of c quarks. At HERA photon gluon fusion is the dominant process for J/ψ production in the kinematic range of $0.3 < z < 0.9$. As already mentioned boson gluon fusion is the leading order contribution to the pointlike component. In next to leading order calculations, processes where the gluon radiates a second gluon which interacts with the photon are included in the pointlike component (see figure 2.4 a). Some other NLO contributions are a second radiated gluon or photon quark interaction with a radiated gluon.

In general the produced quark-antiquark pair is not in a bound state. The transition to a bound state such as the J/ψ meson for c-quarks is described in different models, the color singlet model, the color octet model and the color evaporation model (see sections 2.3.1, 2.3.2 and 2.3.3).

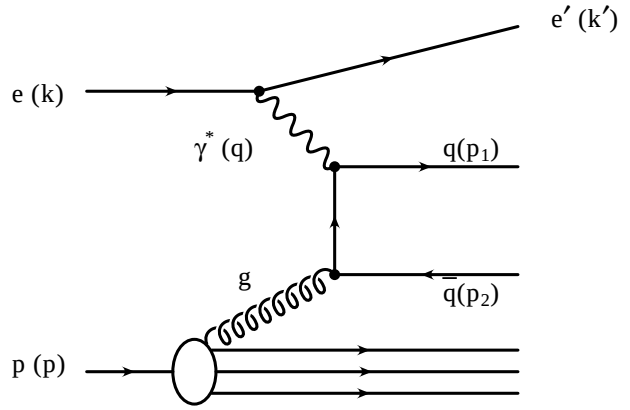

Figure 2.3: Diagram for the production of a quark antiquark pair via boson-gluon fusion.

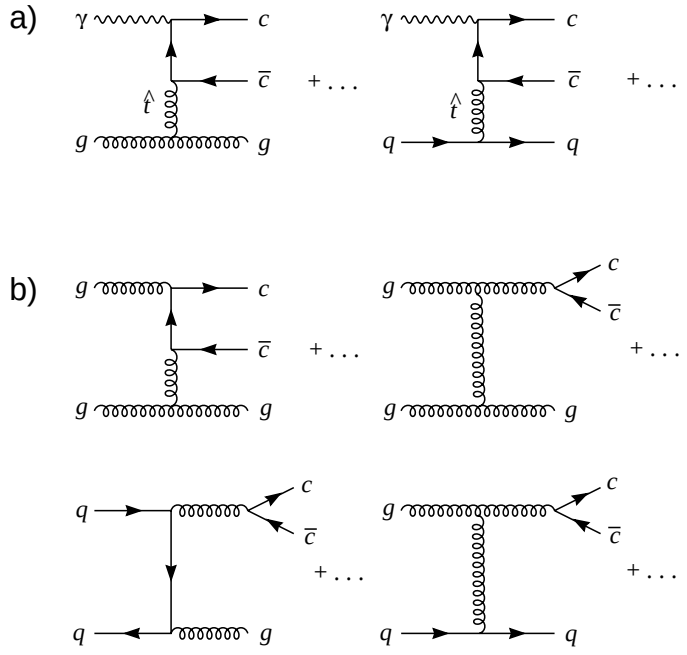

Figure 2.4: $O(\alpha_{em}\alpha_s^2)$ processes contributing to a) pointlike and b) hadronic charmonium photoproduction. $\hat{t}$ is the momentum fraction transfered from the incoming parton (gluon, quark) to the interacting gluon (parton).

2.2.2 Hadronic J/ψ-Production

In addition to the processes where the photon of the electron interacts directly with the parton of the proton there are hadronic (resolved) contributions. A quasi-real photon ($Q^2 \to 0\,\mathrm{GeV}^2$) can behave like a hadron and interact via its partonic contents with the proton. The photon can evolve into quark pairs. In that case one of the two quarks or a radiated gluon participates in the interaction. Therefore the hadronic contributions to J/ψ production are derived from the following interactions:

- quark gluon
- gluon gluon
- quark quark

The generic diagrams for J/ψ meson production in hadronic photon processes are shown in figure 2.4 b. A parton from the proton and a parton from the photon interact in next to leading order in α_s via a virtual quark line or direct. The distributions of the hadronic contents of the photon can be described by parton density functions (PDF). The dominant process is the interaction of two gluons. Hadronic photon events have a second hadronic system besides the proton remnant, the *photon remnant*.
The total ep cross section is composed of the sum of pointlike and hadronic contributions:

$$\sigma_{ep} = \sigma_{ep}[pointlike] + \sigma_{ep}[hadronic]. \tag{2.11}$$

The separation of these two contributions must be handled with care since some terms of the hadronic processes may already be included in the pointlike terms (photon PDF), see section 2.3.3 and [NDE]. Some diagrams for hard subprocesses especially in next to leading order may have their origin in both pointlike and hadronic production processes and thus can lead to double counting.

2.3 Models for J/ψ Production

The three main models describing J/ψ production have one basic assumption in common. They are all based on the factorization of the production process. At first the $c\bar{c}$ pair is produced in a process calculable in perturbative QCD and depending on the production process, i.e. ep or pp etc. Thereafter the $c\bar{c}$ pair develops into the bound state, the J/ψ meson, via a process that is in general not calculable in perturbative QCD and independent of the production process. The factorization is considered legitimate because of the two different time scales of the processes, the $c\bar{c}$ pair is produced on a short time scale of order $1/m_c$ and the bound state formation is a long distance process with time scale of $1/\Lambda_{QCD}$. Λ_{QCD} is the QCD scale.

2.3.1 The Color Singlet Model

The Color Singlet Model (CSM) developed by E. L. Berger and D. Jones in 1980 was the first model to provide quantitative predictions for Charmonium production (see figure 2.6 and [BeJ,BaR]). It is applicable to a variety of processes like hadron collisions, photoproduction and e^+e^- collisions.
The cross section for J/ψ production can be factorized into the short distance cross section of the $c\overline{c}$ pair production calculable in pQCD and the long distance matrix element to describe the non-perturbative formation of the bound state. This is the factorization argument introduced above. The production of a J/ψ in the color singlet model is illustrated in figure 2.5 a). A virtual photon and a gluon fuse via a virtual quark line. A hard gluon has to be emitted in the hard subprocess to be able to produce a $c\overline{c}$ pair with the quantum numbers described below. The differential cross section can thus be written as:

$$\mathrm{d}\sigma(A+B \longrightarrow J/\psi + X) = \mathrm{d}\sigma_{short}(A+B \longrightarrow c\overline{c}(\underline{1},^3S_1) + X) \cdot |R_{J/\psi}(0)|^2. \tag{2.12}$$

A and B are two incoming partons such as γ and p, $\sigma_{short}(A+B \longrightarrow c\overline{c}(\underline{1},^3S_1)+X)$ is the short distance cross section to produce a $c\overline{c}$ in the state $(\underline{1},^3S_1)$ where the $\underline{1}$ denotes a color singlet state. The $^3S_1$ is the $^{2S+1}L_J$ state describing the angular momentum state of the $c\overline{c}$ pair with S, L and J being the quantum numbers of the total spin, the orbital angular momentum and the total angular momentum. $R_{J/\psi}(0)$ is the J/ψ wave function at the origin since the $c\overline{c}$ is in the $(\underline{1},^3S_1)$ state. It is related to the electromagnetic width Γ_{ee} of the charmonium:

$$\Gamma(J/\psi \longrightarrow e^+e^-) := \Gamma_{ee} \approx \frac{4\alpha^2}{9m_c^2} \cdot |R_{J/\psi}(0)|^2, \tag{2.13}$$

with m_c denoting the charm quark mass and α the fine structure constant. This is a leading order approximation.
The original formula to describe J/ψ production in the color singlet model was developed by E. L. Berger and D. Jones in [BeJ]. The cross section was calculated to be:

$$\frac{\mathrm{d}\sigma}{\mathrm{d}x}(ep \longrightarrow eJ/\psi + X) = Bm_{J/\psi}^4 G(x) I(x). \tag{2.14}$$

Here $x = \frac{s'}{\hat{s}}$ where s' is the photon-gluon squared center of mass energy and $\hat{s} = W_{\gamma p}^2$. For photoproduction x can be approximated by:

$$x = \frac{1}{ys}\left(\frac{p_T^2}{z(1-z)} + \frac{m_{J/\psi}^2}{z}\right) \tag{2.15}$$

The constant B is given by:

$$B = \frac{8\pi\alpha_s^2\Gamma_{ee}}{3\alpha\, \mathrm{m}_{J/\psi}}. \tag{2.16}$$

$G(x)$ is the gluon density, it can be simple as suggested by counting rules and momentum constraints in [Far] as used in [BeJ]

$$G(x) = \frac{3(1-x)^5}{x}, \tag{2.17}$$

or as applied in the recent parton density function $MRS(A')$

$$G(x) = \frac{2.24(x^{-0.2})((1-x)^{8.52})}{x}. \tag{2.18}$$

The remaining variable I is the leading order matrix element of the color singlet model. It is defined as:

$$I(x) = \frac{2}{(s+\mathrm{m}^2_{J/\psi})^2}\left\{\frac{s-\mathrm{m}^2_{J/\psi}}{s\,\mathrm{m}^2_{J/\psi}} + \frac{2}{s+\mathrm{m}^2_{J/\psi}} ln(s/\mathrm{m}^2_{J/\psi})\right\} + \frac{2(s+\mathrm{m}^2_{J/\psi})}{s^2\,\mathrm{m}^2_{J/\psi}(s-\mathrm{m}^2_{J/\psi})} - \frac{4ln(s/\mathrm{m}^2_{J/\psi})}{s(s-\mathrm{m}^2_{J/\psi})^2}. \tag{2.19}$$

2.3.2 NRQCD or the Color Octet Model

The Color Octet Model (COM) is an extension of the color singlet model in the sense that it also allows $c\overline{c}$ pairs produced in color octet states to develop into J/ψ mesons by emitting soft gluons.
The COM is a factorization approach in non-relativistic quantumchromodynamics, thus often referred to as NRQCD. This approach was first developed by Bodwin, Braaten and Lepage for the prediction of P-wave Charmonium states [BBL]. It is in fact not a model but a theory [BBL1, BrC] because in the limit of high quark masses it reproduces full QCD [Rot]. The color octet model results in the color singlet model when dropping all color octet contributions.
The J/ψ production in the color octet model is sketched in figure 2.5 b). A photon and a gluon interact via a virtual quark line yielding a $c\overline{c}$ pair. Soft gluons are radiated after the hard subprocess for color conservation to enable the formation of the J/ψ meson. The cross section for the color octet model is described by:

$$\mathrm{d}\sigma(A+B \longrightarrow J/\Psi + X) = \sum_n c_n(A+B \longrightarrow c\overline{c}[n]+X)\langle 0|O_n^{J/\Psi}|0\rangle. \tag{2.20}$$

Here A and B again denote two incoming partons. n labels an on-shell $c\overline{c}$ pair in a definite color, spin and angular momentum. The c_n denotes the short distance cross section for a reaction involving two partons A and B in the initial state and two c-quarks in the final state with the quantum numbers of the state n. c_n is completely calculable in perturbation theory. The long distance part described by the matrix elements $\langle 0|O_n^{J/\Psi}|0\rangle$ involves the hadronization of the $c\overline{c}$ pair in the state n into the J/ψ plus additional soft gluons. The long distance matrix elements are not calculable but assumed to be universal and may be extracted from any experiment ([Kra, Fle]). The infinite sum over the states n may be expressed by a double Taylor-expansion in the relative velocity between the two quarks $\vec{v}$ and the strong coupling constant α_s. In the first order approximation the $c\overline{c}$ system is produced in the color singlet state, the color octet contributions are suppressed. Therefore the color singlet model turns out to be the first order approximation of the color octet model in the Taylor expansion ordered in $\vec{v}$ and α_s.

2.3.3 The Color Evaporation Model

The Color Evaporation Model (CEM), based on the 'local hadron parton duality approach', was first developed in 1977 by F. Halzen, S. Matsuda [Ha1] and H. Fritzsch [Fr1]. Due to its

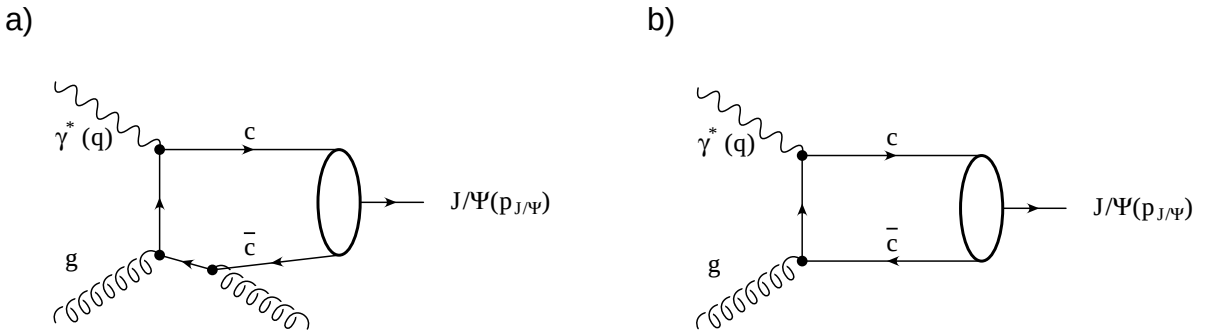

Figure 2.5: Graph for the production of a J/ψ-meson via photon-gluon-fusion: a) in the Color Singlet Model by emitting a hard perturbative gluon, b) in the Color Octet Model by forming a $c\bar{c}$ pair in the color octet state and emitting a soft (nonperturbative) gluon or a photon.

weak predictive power and the poor description of the *z*-distribution (see figure 2.6) the model received little interest and was neglected.

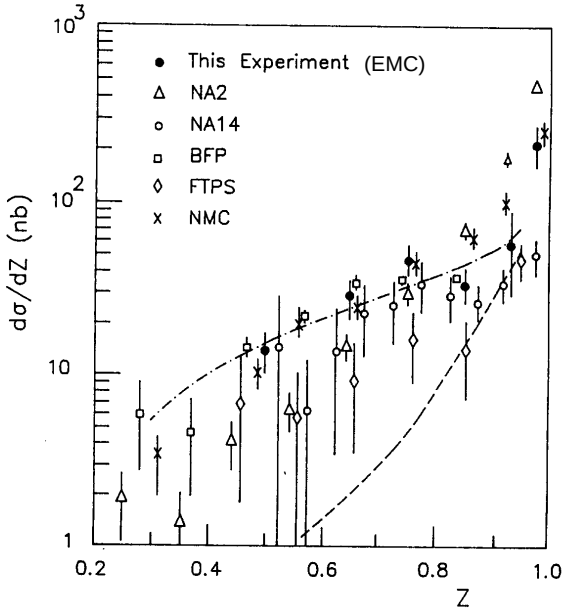

Figure 2.6: $d\sigma/dz$ world data 1992 for inelastic J/ψ production [EMC1]. The dash-dotted curve is the prediction of the color singlet model [BeJ]. The dashed curve from [DuO] is a calculation in leading order of the color evaporation model. The *z* dependence of $d\sigma^2/dz\,dp_T^2$ at $p_T^2 = 1\,\mathrm{GeV}^2$ is plotted. Both curves are arbitrarily normalized.

Recently a group around J. F. Amundson, O. J. P. Eboli, E. M. Gregores and F. Halzen improved the theory [Ha2-8] by including next to leading order processes into their calculations.
The CEM predicts a cross section for the J/ψ production from the cross section of the produced

$c\bar{c}$ pair. It assumes that color can be "bleached" (evaporate) by multiple soft gluon interactions, implying a statistical treatment of color.
The calculation of the total charmonium cross section necessitates the factorization of the two processes, production of the $c\bar{c}$ pair and the formation of the J/ψ. The idea is that all charmonium states and $D\overline{D}$ pairs are produced in the same way and are described by the same distributions, with different normalizations. The cross section for all charmonium and open charm states is given by the two expressions:

$$\sigma_{charmonium} = \frac{1}{9}\int_{2m_c}^{2m_D} \mathrm{d}m_{c\bar{c}} \frac{\mathrm{d}\sigma_{c\bar{c}}}{\mathrm{d}m_{c\bar{c}}} \tag{2.21}$$

and

$$\sigma_{open} = \frac{8}{9}\int_{2m_c}^{2m_D} \mathrm{d}m_{c\bar{c}} \frac{\mathrm{d}\sigma_{c\bar{c}}}{\mathrm{d}m_{c\bar{c}}} + \int_{2m_D}^{\infty} dm_{c\bar{c}} \frac{\mathrm{d}\sigma_{c\bar{c}}}{\mathrm{d}m_{c\bar{c}}} \tag{2.22}$$

$$\simeq \frac{8}{9}\int_{2m_c}^{\infty} \mathrm{d}m_{c\bar{c}} \frac{\mathrm{d}\sigma_{c\bar{c}}}{\mathrm{d}m_{c\bar{c}}}, \tag{2.23}$$

where $\sigma_{c\bar{c}}$ is the parton parton cross section to produce heavy quarks as calculated in standard textbooks (summing up all the possible initial color states and averaging over the final ones, with the color matrices ensuring the appropriate color conservation in the vertices and in the propagators), $m_{c\bar{c}}$ is the invariant mass of the $c\bar{c}$ pair and m_c and m_D are the masses of the c quark and D meson respectively. The factor $\frac{1}{9} = \frac{1}{1+8}$ represents the statistical probability that the $3 \times \overline{3}$ charm pair is asymptotically in a singlet state, the same is valid for the factor $\frac{8}{9}$ and the color octet states.
The factor of $\frac{1}{9}$ for the statistical counting of the formation of color singlet states is explained by W. Buchmüller and A. Hebecker [Bu1], who proposed a description of the formation of rapidity gaps. They suggested that the origin of a rapidity gap corresponds to the $3 \times \overline{3}(= 1 + 8)$ intermediate quark-antiquark state being in a color singlet state and therefore fragmenting independently of the proton remnant. Because color is the source of hadrons, only the color octet states yield asymptotically hadronic states. The mechanism they propose is illustrated in figure 2.7. The diagram represents the production of final state hadrons ordered in rapidity [Ha1].
This leads to the experimentally verified prediction that

$$F_2^{(gap)} = \frac{1}{1+8} F_2. \tag{2.24}$$

Equation 2.24 embodies the conclusion that events with and without gaps are described by the same short-distance dynamics. The appearance of gaps is dictated by non-perturbative final state interactions.
The cross section $\sigma_{charmonium}$ in equation 2.21 is the sum of the cross sections of all possible charmonium states in the mass interval. To determine the cross section for the J/ψ the part $\rho_{J/\psi}$ of $c\bar{c}$ pairs that develop into a J/ψ meson has to be known, leading to:

$$\sigma_{J/\psi} = \rho_{J/\psi}\sigma_{charmonium} \tag{2.25}$$

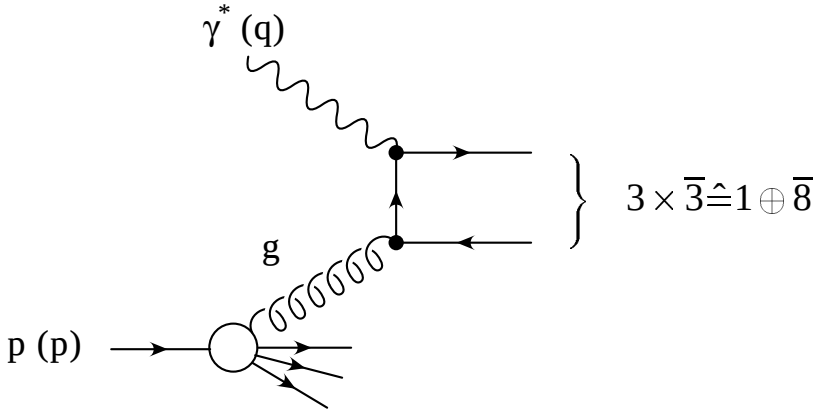

Figure 2.7: Mechanism for the production of rapidity gaps in deep inelastic scattering in a $3 \times \overline{3}$ color state, one color singlet state and eight color octet states.

In a first approximation $\rho_{J/\psi} = \frac{1}{N}$ with N the number of charmonium states below the threshold for the production of two D mesons. This approximation is based on the statistical counting of final states [Ed1], as expected in a scheme with no final state dynamics. A better approximation is

$$\rho_{J/\psi} = \frac{2J_{J/\psi}+1}{\sum_i (2J_i+1)}, \tag{2.26}$$

where J is the spin of any charmonium state i. The sum runs over all charmonium states [Ha2]. The expected value for $\rho_{J/\psi}$ should be a bit larger since phase space corrections favoring the lighter charmonium states are expected. The calculated value is $\rho_{J/\psi} = 0.47$. A fit of the distributions to the data results in a $\rho_{J/\psi}$ between 0.43 (for $MRS(A)$ parton function) and 0.50 (for $GRV-HO$ parton function). The experimentally fitted results for $\rho_{J/\psi}$ are in good agreement with the theoretically calculated one. Predictions with these values applied are shown in figure 2.8 [Ha3]. $\rho_{J/\psi}$ is assumed to be constant and independent of the production process.
The color evaporation model does not explain how the formation of the J/ψ proceeds. It assumes that the open $c\overline{c}$ pair transforms with a certain probability into a bound $c\overline{c}$ pair by soft gluon interactions.
The color evaporation model predicts the same strong maximum in the high z region as the color octet model. The origin is as follows. For $\hat{t} \to 0$, with $\hat{t}$ being the subprocess momentum transfer on the proton side, the gluon exchange diagrams in figure 2.4 represent the QCD evolution of the initial state gluon distribution functions and not higher order gluon exchange diagrams. Therefore the contribution of the gluon exchange diagrams where $\hat{t}$ is soft has already been accounted for by the leading order $\gamma g \to c\overline{c}$ diagram as shown in [NDE]. This double-counting is only relevant for $z \to 1$ and vanishing p_T.
The problem of the peak at high z stems from the evolution of the incoming gluon and not from any feature in the color octet model. A phenomenological factor is introduced in [Ha6] to

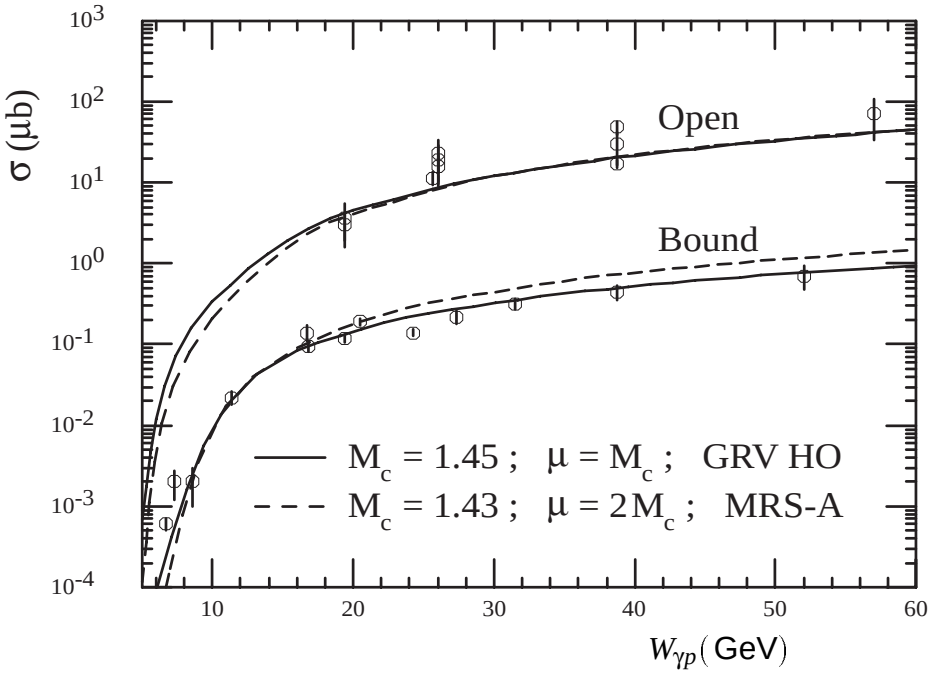

Figure 2.8: Hadroproduction data [Bam] and the cross sections of the color evaporation model at NLO as a function of the photon proton center of mass energy $W_{\gamma p}$ (figure from [Ha3]).

compensate the double counting. The phenomenological correction for the cross section is:

$$\frac{\mathrm{d}^2\sigma}{\mathrm{d}p_T\,\mathrm{d}z} = \big(1 - F(Q_0, p_T)\big)\big(1 - G(Q_0, z)\big)\frac{\mathrm{d}^2\sigma_{c\overline{c}}}{\mathrm{d}p_T\,\mathrm{d}z} \tag{2.27}$$

with

$$F(Q_0, p_T) = e^{-\frac{p_T^2}{k_T^2}} \tag{2.28}$$

and

$$G(Q_0, z) = e^{-\frac{1-z}{z_0 z}}, \tag{2.29}$$

where $k_T^2 = z(Q_0^2 + 4m_c^2) - 4m_c^2$ and $1 - z_0 = \frac{(p_T^2+4m_c^2)}{(Q_0^2+4m_c^2)}$ are positive definite or zero and $\sigma_{c\overline{c}}$ is the cross section for $c\overline{c}$ pair production calculated in perturbative QCD. The parameter Q_0 represents the cut on the t-channel momentum transfer $\hat{t}$ where the higher order diagrams contribute in the low p_T and high z limit. The effect of choosing different values of Q_0 is illustrated in figure 2.10 a) and 2.9. An alternative way of correcting for double counting which yields a similar result is applying a cut of $|\hat{t}| > Q_0^2$. The difference between these two ways of correcting can be seen by comparing figures 2.10 a) and 2.10 b).

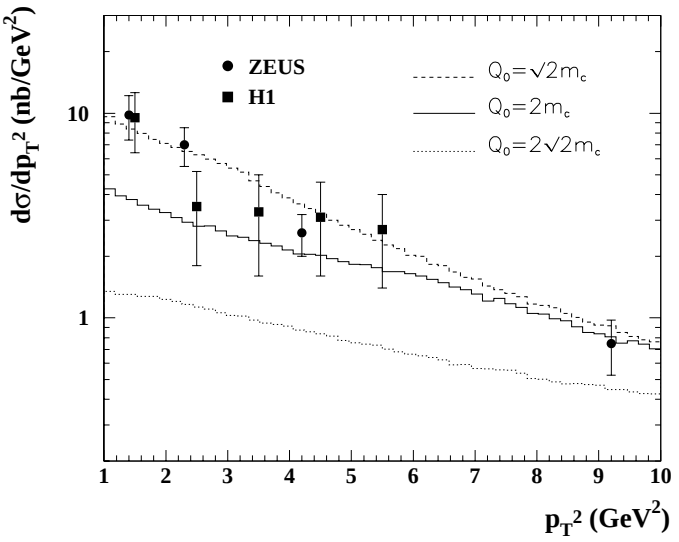

Figure 2.9: H1 and ZEUS data [H1Z] and the CEM γp cross sections as a function of p_T^2 for different Q_0. Cuts of $0.4 < z < 0.9$ and $p_T^2 > 1\,\text{GeV}$ were applied. The GRV structure function with $\Lambda^{(4)} = 300\,\text{MeV}$, renormalization scale $\mu_R = m_c$ and $m_c = 1.3\,\text{GeV}$ was used (figure from [Ha6]). The factorization scale is set to $s'' = x_A x_B W_{\gamma p}^2$ for the subprocess $AB \to J/\psi X$.

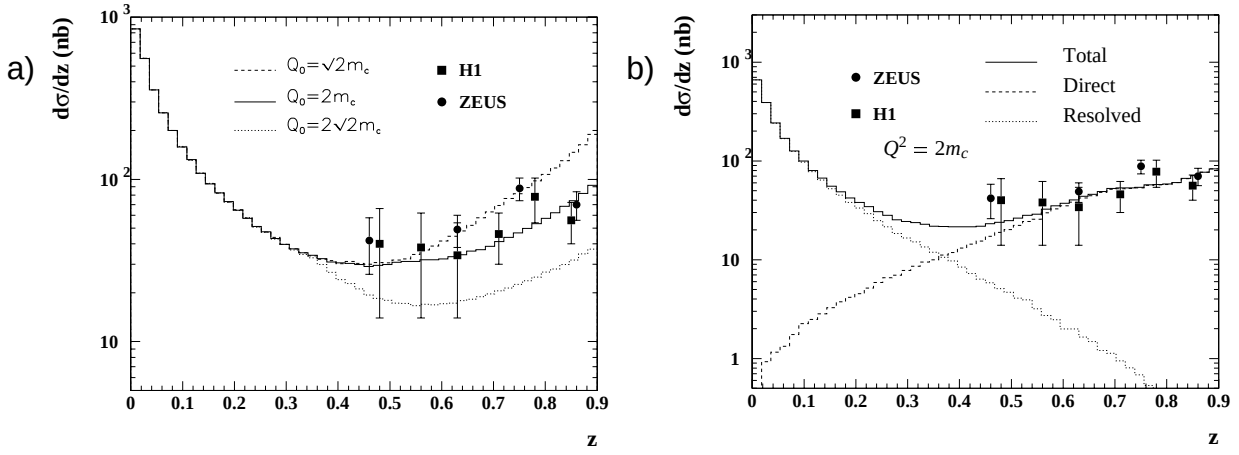

Figure 2.10: γp cross sections as a function of z for the color evaporation model with the correction factor described in the text. In a) the z distribution is shown for three values of the correction factor Q_0. In b) a cut of $|\hat{t}| > Q_0^2 = (2m_c)^2$ was used instead of the correction factor. The remaining parameters of both distributions are the same as in figure 2.9 (figure from [Ha6]).

2.4 Comparison with Experimental Data

In this section a short discussion about the predictions of the three models and comparisons to the data are made.
The color singlet model has a strong predictive power since it has only one non-perturbative parameter for each angular momentum state to be fixed ($R_{J/\psi}$). It describes HERA data for inelastic J/ψ-production for $z < 0.8$. Since in the color singlet model a hard gluon has to be emitted in order to form the J/ψ meson predictions for $0.8 < z < 0.95$ are not reliable. For $z > 0.95$ the J/ψ meson is produced via diffraction.
For TEVATRON data shown in figure 2.11 the color singlet model fails to account for the high production rates. The data are more than one order of magnitude larger than the CSM. In addition the dotted curve for the color singlet cross section is steeper than the data. The color octet model can describe the distribution.

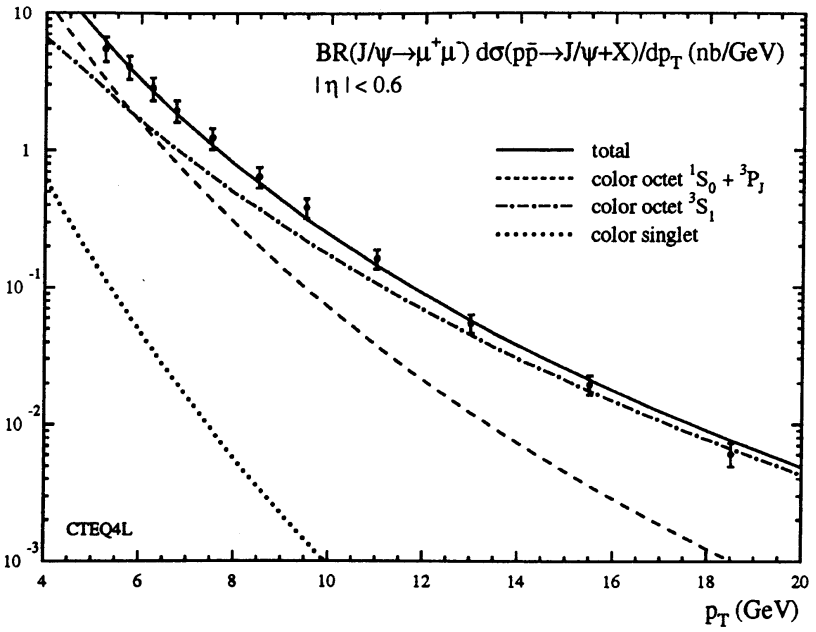

Figure 2.11: p_T distribution for the color singlet model and the color octet model from [Kra1]. The two contributions of the COM add up to the total COM prediction. The CSM predictions are several orders of magnitude smaller than the TEVATRON data.

The color octet model also has a strong predictive power after fixing its universal color matrix elements. It needs an experiment to extract its matrix elements. The matrix elements for the COM were extracted from the TEVATRON data and thus describes these data well. In figure 2.12 it is compared with H1 and ZEUS data. The shaded area indicates the data with their errors. The color singlet model (dashed curve) describes the data, while the color octet model (dotted and dash-dotted curves) peaks for $z \to 1$. It fails to describe HERA data.
The color evaporation model has only weak predictive power. It has only one non-perturbative parameter, $\rho_{J/\psi}$, but it gives no explanation how the transformation into the J/ψ proceeds.

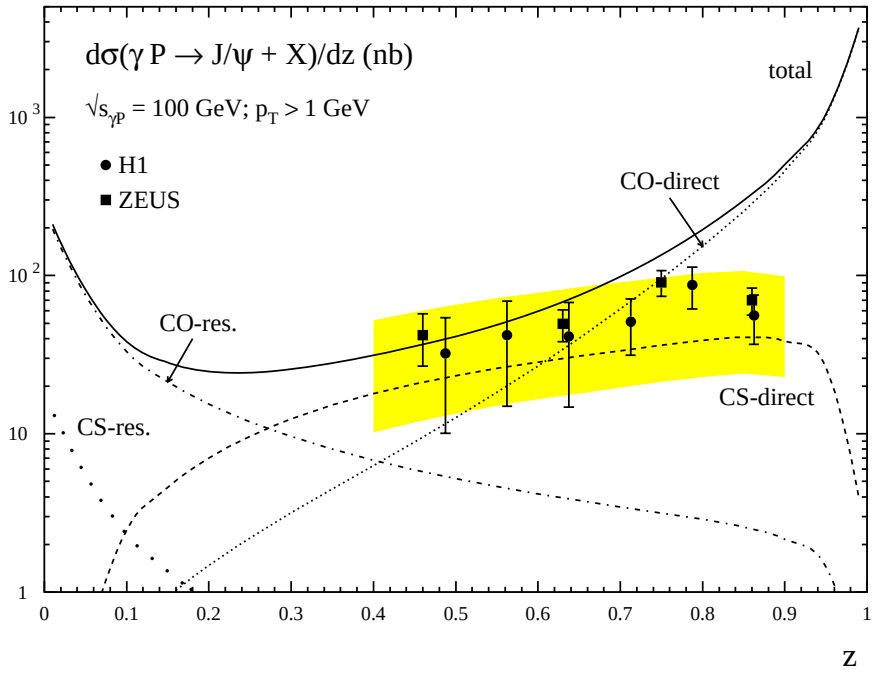

Figure 2.12: HERA data from ZEUS and H1 and the predictions according to the COM and the CSM from [KrB]. The color octet model has a too high cross section for high z.

Nevertheless according to Halzen et al. it seems to fit HERA and TEVATRON data. For the z distributions in figure 2.9 with HERA data the phenomenological correction factor described in the section above was applied. This factor would also reduce the peak for the color octet model in the z distribution. The p_T distribution from the CDF collaboration in figure 2.13 is shown in arbitrary units. The color evaporation model describes the data but shows a slight tendency of a flatter slope.

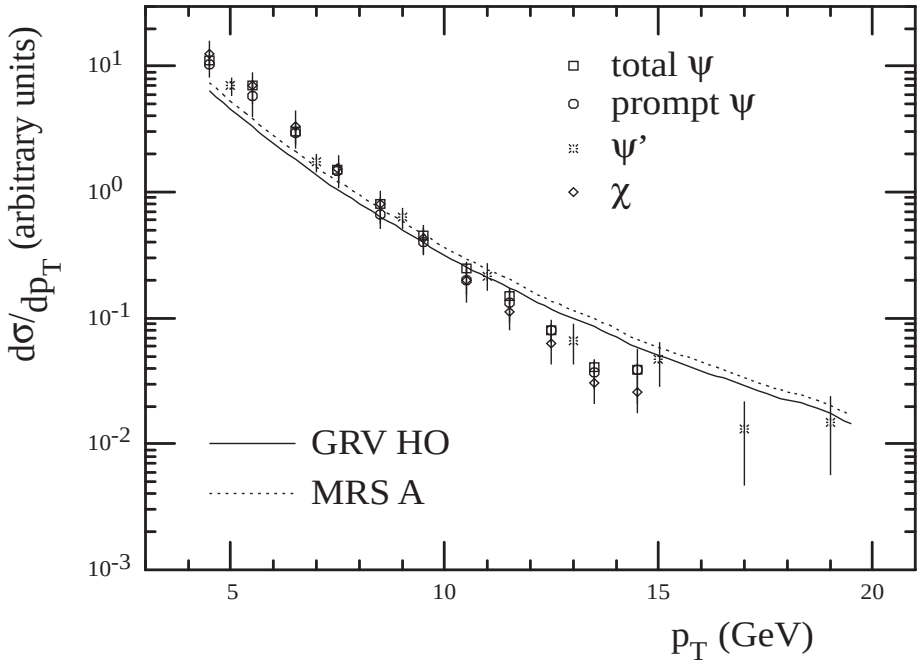

Figure 2.13: Data from the CDF Collaboration [CDF1] shown with arbitrary normalization. The curves are the predictions of the CEM at tree level. The normalization is correctly predicted within a factor of 2.2 (from [Ha3]).

Chapter 3

Monte-Carlo Generators and Theory Programs

In this chapter the programs used to calculate distributions for the present analysis are introduced. At first the two Monte-Carlo generators EPJPSI and RAPGAP are presented. In the second section the FMNR program which is used to calculate open $c\overline{c}$ production is described. RAPGAP and the FMNR program are used for the calculation of the color evaporation model. The scaling factors used by the programs are listed in table A.6 in appendix A.4.

3.1 Monte-Carlo Generators

Monte-Carlo generators (MCs) are used to obtain sets of simulated events that contain full information about both physics processes and detector efficiencies. The MCs generate events according to a distribution that is gained from data or a theory. This procedure is very successful to describe LO distributions but fails to include full NLO contributions since in next to leading order calculations negative weights appear. Most Monte-Carlo generators are able to include next to leading order contributions partially.

3.1.1 EPJPSI: Color Singlet Monte-Carlo Generator

The Monte-Carlo generator EPJPSI [Jun1] was developed to describes the production of J/ψ mesons in several high energy scattering processes namely in ep, μp, γp, pp and $p\overline{p}$ collisions. It is a program to simulate elastic and inelastic vector meson production in photoproduction and deep inelastic scattering. There are five different ways to produce J/ψ mesons, although only photon-gluon fusion in the LO color singlet model (see section 2.3.1) will be used here.
The distribution of the energy of the photon emitted by the electron is described by the Weizsäcker-Williams approximation [WW]. For the partons radiated from the p or γ various parton density functions (PDFs) can be chosen. Initial state parton radiation of gluons and relativistic corrections which account for the relative momentum of the quarks inside the J/ψ

meson can be included in the calculations. In this analysis EPJPSI events were produced in leading order without initial state radiation and without the relativistic corrections. For the fragmentation of the final state the Lund-String-Model, implemented in the program JETSET [Sjö], was used.
Apart from the leading order boson-gluon fusion process J/ψ mesons can be produced in gluon gluon fusion via a virtual quark line by the subprocesses: $gg \to J/\psi g$ and $gg \to J/\psi\gamma$. These hadronic contributions are not included in the leading order color singlet model distributions calculated here.
Only leading order boson gluon fusion contributions were generated. For the gluon density in the proton the parameterization $MRS(A')$ [PDF] was used. The decay products of the J/ψ meson were limited to muons. In H1 analyses a θ-cut of $20^\circ < \theta < 160^\circ$ is applied to the muons in order to limit the events to the central tracking region. This cut will be used in this analysis for the double differential distributions in section 4.3.2. 50 000 J/ψ mesons were simulated leaving 5.834 vector mesons within the θ range for the comparison.
For more detailed settings see section 4.2.3 and the appendix A.1.

3.1.2 RAPGAP: Monte-Carlo Generator for Heavy Quark Production

RAPGAP [Jun2] is a universal Monte-Carlo generator for the production of events in electron proton scattering. Deep inelastic scattering, diffractive and non-diffractive events and events where the photon hadronizes can be simulated. This program also includes the features listed in the above subsection: initial state parton radiation and hadronic photon contributions, i.e. $gg \to c\overline{c}$ and $q\overline{q} \to c\overline{c}$.
As for EPJPSI the parton density parameterization set $MRS(A')$ is used on the proton side. All settings for the RAPGAP and EPJPSI Monte-Carlo generators are the same, except that no angular cut was applied to the RAPGAP events. For a detailed list of the settings see section 4.2.1 and appendix A.2.
While EPJPSI only produces J/ψ mesons RAPGAP is used here to produce open $c\overline{c}$ pair events. The differences between the leading order and next to leading order contributions of the color evaporation model will be analyzed by comparing RAPGAP and FMNR distributions. Therefore RAPGAP was set to exclude most next to leading order contributions.
A cut on the invariant mass of the $c\overline{c}$ pair system of $2m_c < m_{c\overline{c}} < 2m_D$ with $m_c = 1.4\,\mathrm{GeV}$ and $m_D = 1.87\,\mathrm{GeV}$ is made to implement the color evaporation model into the distributions. The $c\overline{c}$ pair distributions calculated by RAPGAP are then normalized to the color evaporation model in the same way as the distributions calculated by the program FMNR, i.e a factor of $\frac{\rho_{J/\psi}}{9}$ is multiplied to the cross sections. The normalization is described in detail in section 4.1.2.

3.2 FMNR: Next to Leading Order Program for Heavy Quark Production

Unlike EPJPSI and RAPGAP the "FMNR" program is not a Monte-Carlo generator. It was developed by S. Frixione, M. L. Mangano, P. Nason and G. Ridolfi. FMNR will be used to

calculate the next to leading order color evaporation model cross sections. In contrast to the Monte-Carlo generators this program does not generate events according to a theoretical prediction but randomly generates events. These events are weighted with the theoretical distribution. FMNR [FMNR1,5,10] is a program to calculate next to leading order heavy quark-antiquark pair production in QCD. The program can either be run in LO or in NLO mode to calculate the cross section for any heavy quark-antiquark pair in either photon-proton or electron-proton collisions. For photon-proton collisions the photons collide with the protons with the same center of mass energy for all events (monochromatic photon beam). The electron-proton collisions are simulated by photon-proton collisions where the photon beam has an energy spectrum calculated in the Weizsäcker-Williams approximation by the formula given in [FMNR2] (see equation 2.8).
The program FMNR is separated into two different program packages, one to calculate the pointlike contributions of the cross section and the other to calculate the hadronic contributions. The pointlike and hadronic components have to be added in order to yield results which can be compared to the data in the whole kinematic region. For both contributions there are three sets of distributions that can be calculated: single inclusive distributions ($\frac{d\sigma}{dp_T}$, $\frac{d\sigma}{dy}$), double differential distributions (”correlations”, $\frac{d\sigma^2}{dp_T\,dz}$) and total cross section (total cross section, $\frac{d\sigma}{dx_{partons}}$). It is also possible to choose the classes of diagrams contributing to the cross section, either leading order (Born level) or next to leading order, see table 3.1.

	Born level (LO)	NLO
pointlike	$\alpha_{em}\alpha_s$	$\alpha_{em}\alpha_s^2$
hadronic	α_s^2	α_s^3

Table 3.1: Classes of diagrams being evaluated for Born and NLO contributions in powers of α_{em} and α_s.

For the pointlike component the radiation of a photon from the electron is described in the Weizsäcker-Williams approximation [WW, FMNR2]. On the proton side the parton density functions (PDFs) are used. For the pointlike component the program independently calculates the contributions from the following initial states:

- photon gluon fusion
- photon quark or photon antiquark interaction

Each of these contributions can be included or excluded separately.
For the hadronic component parton density functions are used on the proton side. The hadronization of the photon is described by the photon structure functions. For electron proton collisions the radiated photon on the electron side is again described by the Weizsäcker-Williams approximation. Therefore the Weizsäcker-Williams approximation and the photon structure functions are combined to ’electron PDFs’. For the hadronic component the program independently calculates the contributions from the following initial states:

- gluon gluon fusion
- antiquark quark or quark antiquark interaction
- gluon quark or gluon antiquark or quark gluon or antiquark gluon interaction

Each of these contributions can again be included or excluded separately.
For the present analysis the hadronic and pointlike contributions were used in next to leading order. For the comparison with the leading order Monte-Carlo generator RAPGAP (see section 4.2.1) and with the Monte-Carlo generator EPJPSI the contributions are restricted to the pointlike component. As for the Monte-Carlo generators $MRS(A')$ was used to describe the parton density distributions on the proton side. For the hadronic part of the photon $GRV-HO$ was used as the parton density distribution. The photonflux is implemented via the Weizsäcker-Williams function. For the complete settings refer to chapter 4 and appendix A.3.

Chapter 4

Results

As already seen the color singlet model fails to describe the high production rates at the TEVATRON and the color octet model fails to describe HERA data. It is desired to describe all data with only one theory in order to understand the production process of charmed mesons. Therefore further investigations in the models have to be pursued.
In this chapter the color evaporation model will be analyzed and results of different programs will be compared with each other and with the data. In section 4.1 results from the program of the theory group FMNR will be compared with published results by its authors Frixione et al. The program is then used to calculate the expectations for p_T^2, $W_{\gamma p}$ and z in the color evaporation model. The next to leading order contributions of the CEM are investigated. In section 4.2.1 the leading order predictions simulated by the Monte-Carlo generator RAPGAP are compared with the next to leading order distributions calculated by the FMNR program. In section 4.2.2 a comparison of the color evaporation model results calculated by the FMNR program and the results of Halzen et al. is made.
In section 4.2.3 distributions of the color singlet model Monte-Carlo generator EPJPSI are generated and compared with the predictions of the FMNR program. The same three relevant variables, p_T^2, $W_{\gamma p}$ and z are plotted in sections 4.2.1-4.3.
At last HERA data will be compared to the color evaporation model predictions calculated by the FMNR program. In addition to the distributions of p_T^2, $W_{\gamma p}$ and z, p_T^2 will be investigated in four different z-bins.
In this chapter photoproduction will be investigated. Therefore a cut of $Q^2 \leq 1\,\mathrm{GeV}$ is applied to all distributions.

4.1 The FMNR program

In this section the FMNR program is studied which calculates cross sections for $c\overline{c}$ production. It is shown how the color evaporation model is implemented using this program and how different cuts affect the $c\overline{c}$ pair cross sections.

4.1.1 Validating the FMNR program

First several tests are made in order to verify the correct usage of the program. For a variety of settings the calculated cross sections are compared with the cross sections published by the authors of the FMNR program [FMNR6,7]. These are listed in table 4.1. It is found that the cross sections are in good agreement for different parton density functions (PDF), charm masses, center of mass energies and renormalization scales in photon-proton collisions as well as in electron-proton collisions for both the pointlike and hadronic components. For the latter $MRS(A')$ was used for the proton PDF for all cross sections. For the calculation of the cross section the program was run in the 'total cross section' mode as described in [FMNR10], see also chapter 3.2.

Component	Type	Proton PDF	m_c [GeV] m_c	μ_R	$W_{\gamma p}$ [GeV]	FMNR published	this analysis
pointlike	γp	MRS(A)	1.5	m_c	100	2.826 μb	2.839 μb
pointlike	γp	CTEQ 2MF	1.5	m_c	100	2.425 μb	2.491 μb
pointlike	γp	MRS D-'	1.2	$\frac{m_c}{2}$	30	2.363 μb	2.376 μb
pointlike	γp	MRS D-'	1.5	$\frac{m_c}{2}$	280	14.79 μb	14.90 μb
hadronic	γp	GRV-HO	1.5	m_c	100	0.673 μb	0.679 μb
hadronic	γp	LAC1	1.8	$2m_c$	280	5.283 μb	5.309 μb
pointlike	ep	MRS(A)	1.5	m_c	314	0.605 μb	0.581 μb
pointlike	ep	CTEQ 2MF	1.5	m_c	314	0.535 μb	0.525 μb
hadronic	ep	GRV-HO	1.5	m_c	314	0.129 μb	0.130 μb
hadronic	ep	LAC1	1.8	m_c	314	0.196 μb	0.196 μb

Table 4.1: Pointlike and hadronic component of the $c\bar{c}$ pair production cross section for γp and ep collision with various settings in comparison with the data published in [FMNR6, FMNR7].

Further investigations are made in order to show that also the distributions are reproduced. In figure 4.1 the p_T distribution published in [FMNR7] is compared with the p_T distribution reconstructed by the theory program (in 'single inclusive' mode). The two figures display the transverse momentum distribution for the contributions of the pointlike and hadronic components and for the sum for a cut on the rapidity of $|\eta| < 1.5$. They show a reasonable agreement. The reproduced p_T distribution shows a somewhat higher cross section in general. No explanation for this effect was found, all the settings for the reproduced cross section are the same as in the publication.

4.1.2 Calculation of the Color Evaporation Model

Several steps have to be made in order to calculate the expectation of the color evaporation model cross sections for J/ψ production. For this purpose the $c\bar{c}$ pair cross section is integrated

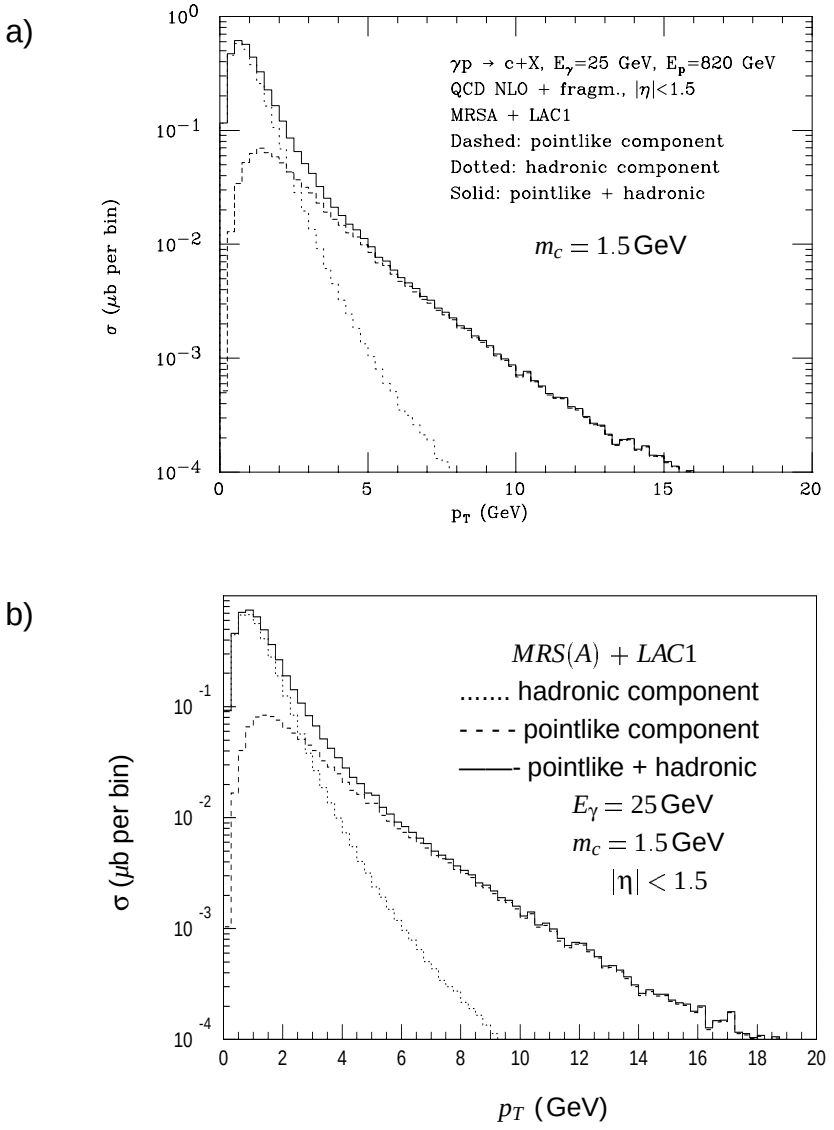

Figure 4.1: γp cross sections as a function of the transverse momentum of the charm quarks. The pointlike and hadronic contributions are separately shown, together with the sum of the two. a) displays published FMNR results (figure from [FMNR7]) and b) shows the reproduced distribution. The same settings are used for both distributions.

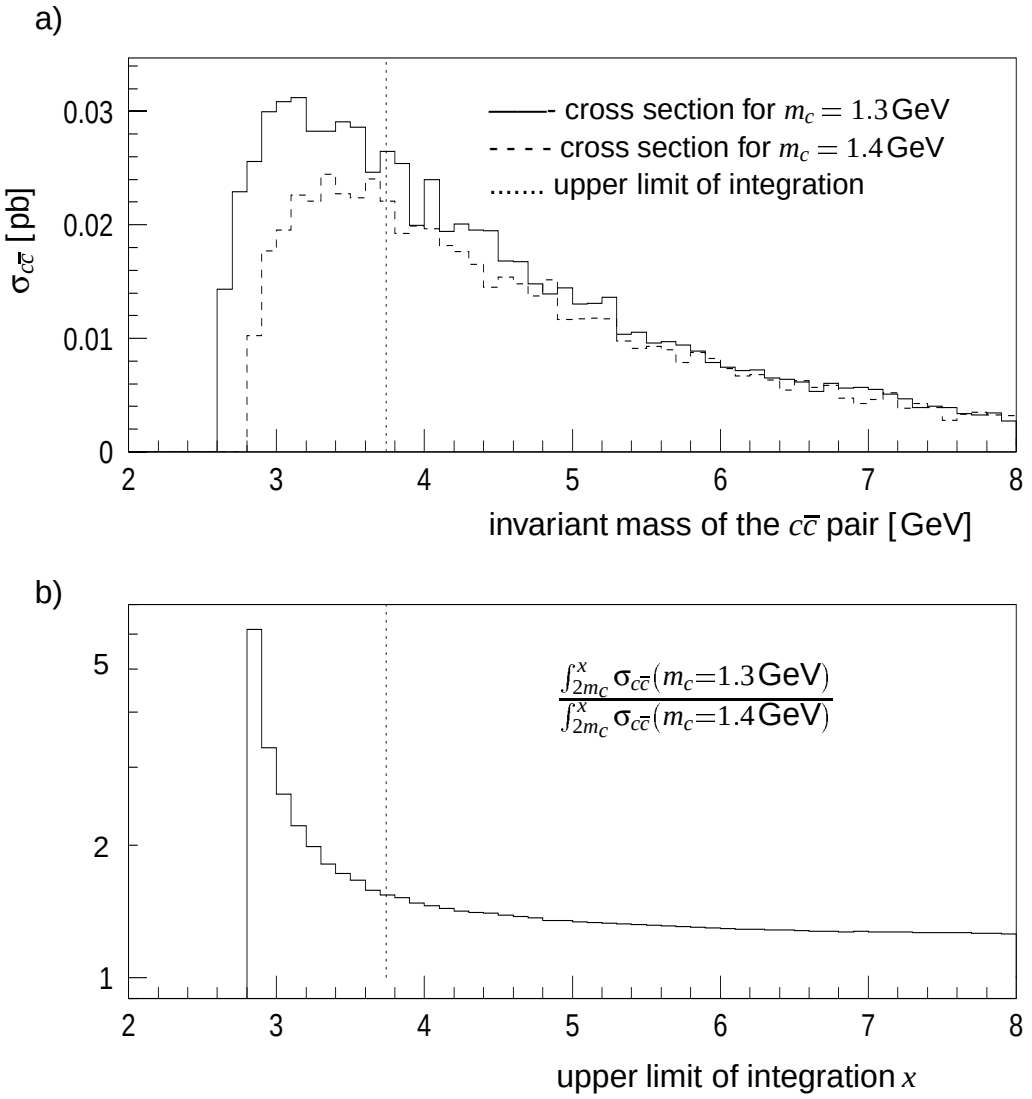

Figure 4.2: a) ep cross section as a function of the invariant mass of the $c\bar{c}$ pair. The point-like and hadronic component as calculated by the FMNR program for $m_c = 1.3\,\mathrm{GeV}$ (solid line) and $m_c = 1.4\,\mathrm{GeV}$ (dashed line) are shown. For the color evaporation model only contributions from $2m_c \leq m_{c\bar{c}} \leq 2m_D = 3.74\,\mathrm{GeV}$ are taken into account. The upper cut is indicated by the dotted line. b) The integral over the cross section for $m_c = 1.3\,\mathrm{GeV}$ divided by the integral over the cross section for $m_c = 1.4\,\mathrm{GeV}$ with the upper limit of the integral on the x-axis.

over the invariant mass of the $c\bar{c}$ pair between $2m_c$ and $2m_D$ (see chapter 2.3.3 equation 2.21). This is done by limiting the invariant mass to that energy region. The cross section as a function of the invariant mass of the $c\bar{c}$ pair is plotted in figure 4.2 a) for two different charm masses. The charm masses of $m_c = 1.3\,\mathrm{GeV}$ and $m_c = 1.4\,\mathrm{GeV}$ are chosen since in the publications of Halzen et al. those charm masses are used frequently [1]. It can be seen that the distributions have a very similar shape, they peak at low energies and then decrease approximately like $\frac{1}{x}$. The

[1] From now on $m_c = 1.4\,\mathrm{GeV}$ will be used unless specified otherwise.

cross section for a higher charm mass is lower than for the charm mass $m_c = 1.3\,\text{GeV}$ and its peak is shifted to higher energies. Therefore the two distributions greatly differ in the integrated region. The lower threshold for the integration, the shifted peak and the different height of the distributions indicate that the color evaporation model is very sensitive to the charm mass. A factor of two can easily be accounted for by choosing a different mass m_c. In figure 4.2 b) the fraction of the integral over the cross section for $m_c = 1.3\,\text{GeV}$ of the integral over the cross section for $m_c = 1.4\,\text{GeV}$ is shown. It shows a strong sensitivity for the upper limit of the integration as well, the larger the region integrated the smaller the factor between the two cross sections. For the two values of the charm masses the cross section integrated up to the upper limit of $2m_D = 3.74\,\text{GeV}$ differs by a factor of ≈ 1.6.
In addition to the integration over the invariant mass the cross section has to be normalized as described in chapter 2.3.3 to calculate the color evaporation model cross sections. A normalization factor of $N = \frac{\rho_{J/\Psi}}{9}$ (see equations 2.21 and 2.26) is applied [2].
Both the pointlike and the hadronic component have to be considered to compare the color evaporation model predictions with the data. Since FMNR calculates cross sections for either monochromatic photon beams or an electron beam of a given energy colliding with a proton (see section 3.2) the latter one was chosen for the pointlike component. The hadronic component was calculated using the monochromatic γp option of the FMNR program because it is not possible to retrieve any information about y and thus $W_{\gamma p}$ and z in the hadronic part of the FMNR program when run in ep mode. Since FMNR allows only monochromatic photon beams for γp cross sections it was run for several beam energies to generate a distribution of photon energies. In order to determine the hadronic component in ep cross sections FMNR was run for twenty $W_{\gamma p}$ bins of 10 GeV width from 60 GeV to 260 GeV. The twenty contributions were then multiplied by the photonflux in each $W_{\gamma p}$ bin and added.

4.1.3 The Effects of Kinematical Cuts

In this subsection the influences of different kinematical cuts on the distributions of p_T^2, z and $W_{\gamma p}$ are investigated.
In figure 4.3 the cross section as a function of p_T^2 and z are displayed for different cuts which are also indicated in the figure. In figures 4.3 a) and b) the solid line is the cross section for $c\overline{c}$ production without any cuts applied. For the p_T^2 distribution it shows a peak at low p_T^2 and a decreasing cross section for higher p_T^2. The first bin is negative and can therefore not be shown on a logarithmic scale. The negative value is a result of the singularity in next to leading order contributions at $p_T^2 = 0$. This is discussed in [FMNR1] and section 4.3.2. The z distribution shows a strong peak for $z \to 1$ and a second maximum in the cross section for $z \to 0$.
In figure 4.3 a) and b) the dashed line shows the $c\overline{c}$ pair cross section with a cut in the invariant mass of the $c\overline{c}$ pair of $2m_c = 2.8\,\text{GeV} \leq m_{c\overline{c}} \leq 2m_D = 3.74\,\text{GeV}$. As expected the cross section decreases when the mass cut is applied due to the smaller phasespace considered. In addition the p_T distribution appears slightly steeper. The z distribution has the same shape as the one without cuts.
The dash-dotted line has the cut on the mass interval and a cut on the angle of the charm quarks

[2] These normalizations and the integration over the invariant mass will be included for all distributions of the FMNR program in sections 4.2.1-4.3.2 in order to represent the color evaporation model.

of $20^\circ < \theta_c < 160^\circ$. The angle θ_c is assumed to correlate with the angle θ_μ of the decay-muons of the J/ψ meson. Since FMNR is only calculating open $c\bar{c}$ pair production no decay products of the J/ψ are available. The behavior of the p_T and z distributions for the θ_c cut is of special interest because at the H1 experiment standard analysis cuts include a cut in the central detector region of $20^\circ < \theta_\mu < 160^\circ$ for muon track reconstruction. The p_T^2 distribution shows no change in shape but a lower cross section than without the cut. The z distribution however shows a completely different behavior for low z. The low z region is suppressed efficiently by the cut on θ (dash-dotted line). For this reason a z cut of $0.3 \leq z$ was applied to the data and the color evaporation model. A cut of $z \leq 0.9$ was also applied.
A cut on $p_T^2 \geq 1\,\mathrm{GeV}^2$, the mass cut, the z cut and a cut on the photon proton center of mass energy of $60\,\mathrm{GeV} \leq W_{\gamma p} \leq 180\,\mathrm{GeV}$ are applied to the dotted lines in figure 4.3 a) and b). For the p_T^2 distribution the cut on p_T^2 and for the z distribution the cut on z are not applied in order to see the shape of the distributions outside the cuts. The peaks of the dotted line are less pronounced for both, the p_T^2 distribution at low p_T^2 after the z cut and the high z region for the z distribution after the p_T^2 cut. This implies a correlation between these two regions. The cuts applied to the dotted line are used in the present analysis for the data as well.
In figure 4.4 the same distributions as in figure 4.3 are plotted. In addition to the total cross section the pointlike and hadronic contributions are indicated by dashed and dotted lines respectively. The partitions a-d indicate the different cuts made. Figure 4.4 a) is without a cut, b) with the cut on the invariant mass interval, c) with the additional θ_c cuts and d) has the mass cut, the p_T^2 cut, the z cut and the $W_{\gamma p}$ cut applied. The p_T^2 and z cuts are again not applied to the p_T^2 and z distributions respectively but indicated by dotted lines. The first column shows the p_T^2 distributions, the middle column the $W_{\gamma p}$ distributions and the column on the right hand side the z distributions. Here it can be seen that the hadronic contribution is responsible for the peak at low z and the pointlike component for the peak at high z. In figure 4.4 c) it can be seen that the hadronic component is suppressed by the θ_c cut. After applying the z cut in the analysis the hadronic contribution to the total cross section will be only a few percent.

4.2 Comparison of the FMNR Predictions with other Calculations

In this section the color evaporation model as calculated with the FMNR program is compared with other calculations. At first the next to leading order predictions of the FMNR program are compared with the predictions of the leading order Monte Carlo generator RAPGAP, which is used to calculate the color evaporation cross sections. Then a comparison with the predictions of Halzen et al. is made. Subsequently the cross sections as calculated with the FMNR program are compared with the color singlet Monte Carlo generator EPJPSI. At last the color singlet cross section as predicted by E. L. Berger and D. Jones are compared with the cross sections calculated by EPJPSI and the FMNR program.

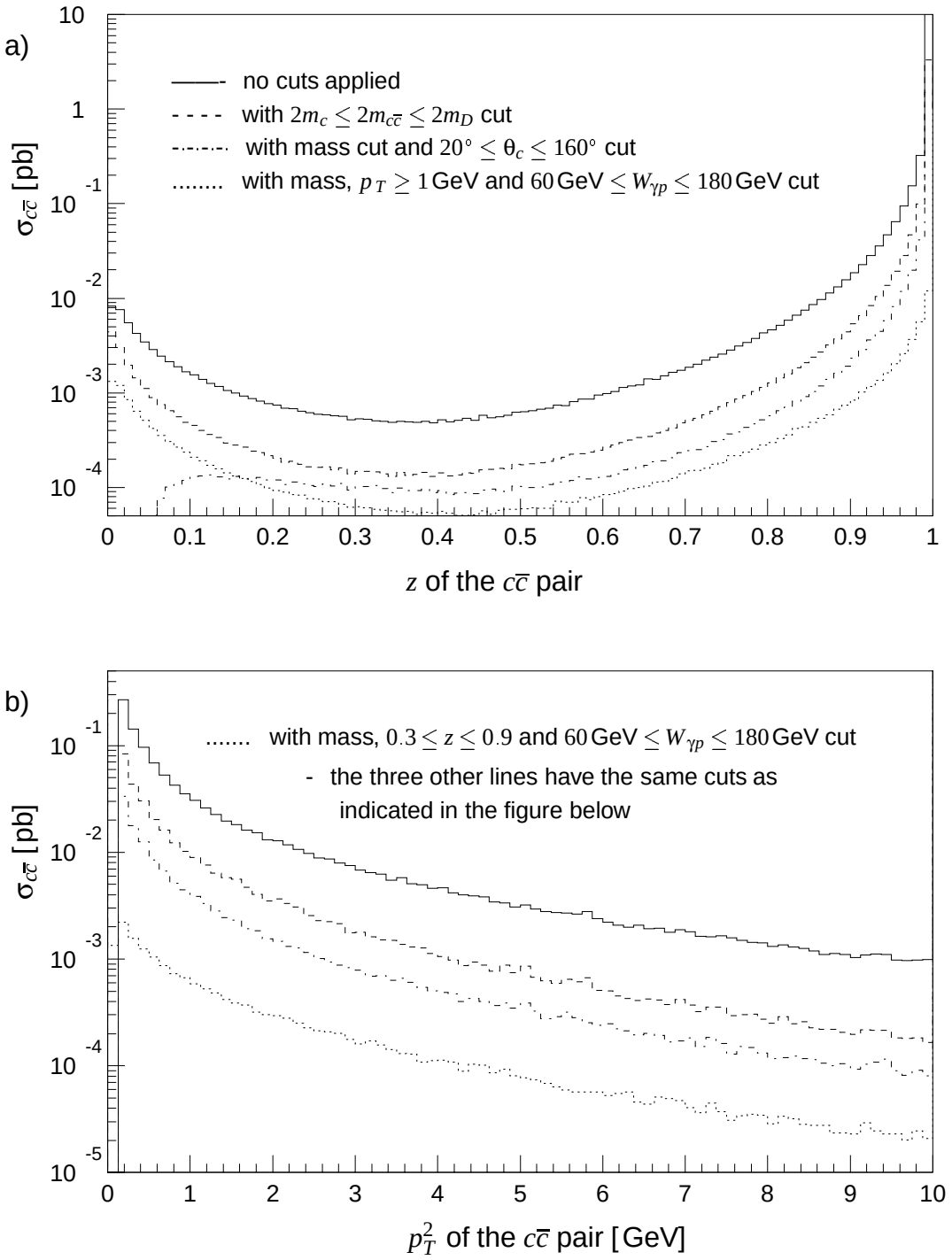

Figure 4.3: ep cross sections from the FMNR program including the pointlike and the hadronic contributions as a function of a) z and b) p_T^2 for different cuts as indicated in the legend. $MRS(A')$ was used as proton PDF and $GRV-HO$ as photon PDF. A charm mass of $m_c = 1.4\,\text{GeV}$ was used. For b) the cuts are described in a), only the dotted line corresponds to the cuts indicated.

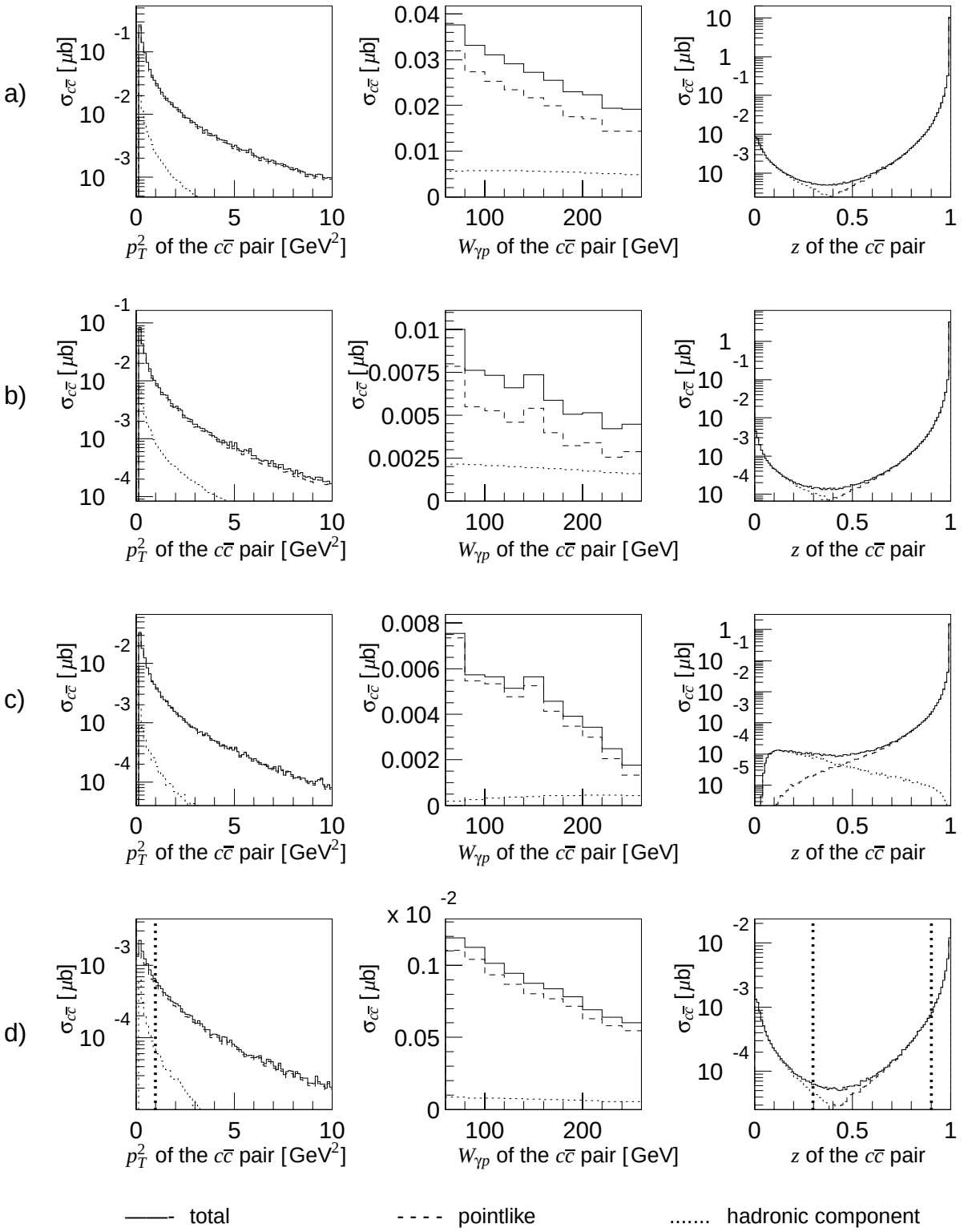

Figure 4.4: *ep* cross sections as a function of p_T^2, $W_{\gamma p}$ and z as calculated by the FMNR program with $MRS(A')$ as proton PDF, $\sqrt{s} = 300\,\text{GeV}$ and $m_c = 1.4\,\text{GeV}$. The dashed line shows the contributions of the pointlike component and the dotted line represents the hadronic contributions. The solid line is the total $c\bar{c}$ cross section. Different cuts were applied: **a)** no cuts; **b)** $2m_c \leq m_{c\bar{c}} \leq 2m_D$; **c)** $2m_c \leq m_{c\bar{c}} \leq 2m_D$ and $20^\circ \leq \theta_c \leq 160^\circ$; **d)** $2m_c \leq m_{c\bar{c}} \leq 2m_D$, $p_T^2 \geq 1\,\text{GeV}$, $0.3 \leq z \leq 0.9$ and $60\,\text{GeV} \leq W_{\gamma p} \leq 180\,\text{GeV}$. The p_T^2 and z cut were however not applied to the p_T^2 and z distributions respectively. The positions of the cuts are indicated by the dotted lines.

4.2.1 Comparison of Leading and Next to Leading Order Predictions of RAPGAP and the FMNR Program

It has been shown in figure 2.6 that the leading order predictions of the color evaporation model are not fully capable of describing the data. In this chapter the color evaporation model will be investigated. The next to leading order predictions calculated by FMNR are compared with the leading order distributions simulated by the RAPGAP Monte-Carlo generator (described in chapter 3.1.2). This cross check is made to gain a better understanding of the NLO contributions of the color evaporation model.
RAPGAP can be used in many different modes, for the present purpose it will be used to calculate open $c\overline{c}$ pair cross sections. Since FMNR calculates cross sections for open $c\overline{c}$ pair cross sections too, the RAPGAP distributions are integrated over the mass range of $2m_c \leq m_{c\overline{c}} \leq 2m_D$ and normalized as done for the FMNR program (see chapter 4.1) in order to describe the color evaporation model predictions.
For RAPGAP and FMNR only the pointlike components are simulated and compared. The contributions of the hadronic and pointlike components to the next to leading order distributions of the FMNR program can be seen in figure 4.4.
In leading order boson gluon fusion the relations $p_T^2 = 0$ and $z = 1$ hold for all events. This can be seen when running FMNR at Born level and will not be shown here. RAPGAP is anticipated to extend to higher values of p_T^2 and to values below one for the z distribution. Expectations for the NLO distributions are a generally higher cross section due to more processes contributing and flatter p_T^2 and z distributions.
In figure 4.5 the next to leading order distributions calculated by FMNR and the leading order distributions calculated by RAPGAP are shown for p_T^2, $W_{\gamma p}$ and z. The NLO distributions are shown as a solid line and the LO distributions are displayed by the shaded area. It can be seen that the FMNR distributions greatly differ from the RAPGAP distribution. For $p_T^2 \to 0$ a peak is observed for both distributions. The leading order cross section however shows a more pronounced peak: the shaded RAPGAP distribution is strongly peaked for $p_T^2 \to 0$. The NLO distribution shows a long tail towards high p_T^2. For the lowest p_T^2 bin the next to leading order calculation leads to large negative weights and thus a negative value for the cross section. This can not be shown on a logarithmic scale. The negative contribution for low p_T^2 in next to leading order was already observed in [FMNR1] and is discussed there. For $W_{\gamma p}$ the distribution (see figure 4.5 b) has a range from $0 - 300\,\mathrm{GeV}$. Here again the RAPGAP distribution has a lower cross section than the FMNR distribution. Both peak for a $W_{\gamma p} \approx 10 - 15\,\mathrm{GeV}$ but the NLO maximum appears shifted to lower $W_{\gamma p}$. The z distributions are displayed in the third part of the figure. Again the RAPGAP distributions have a generally lower cross section and show a stronger peak for $z \to 1$. As for the p_T^2 distribution the NLO z distribution covers a wider range of z than the LO one. As expected the pointlike next to leading order distributions show a higher cross section and a wider p_T^2 and z range than the leading order distributions.

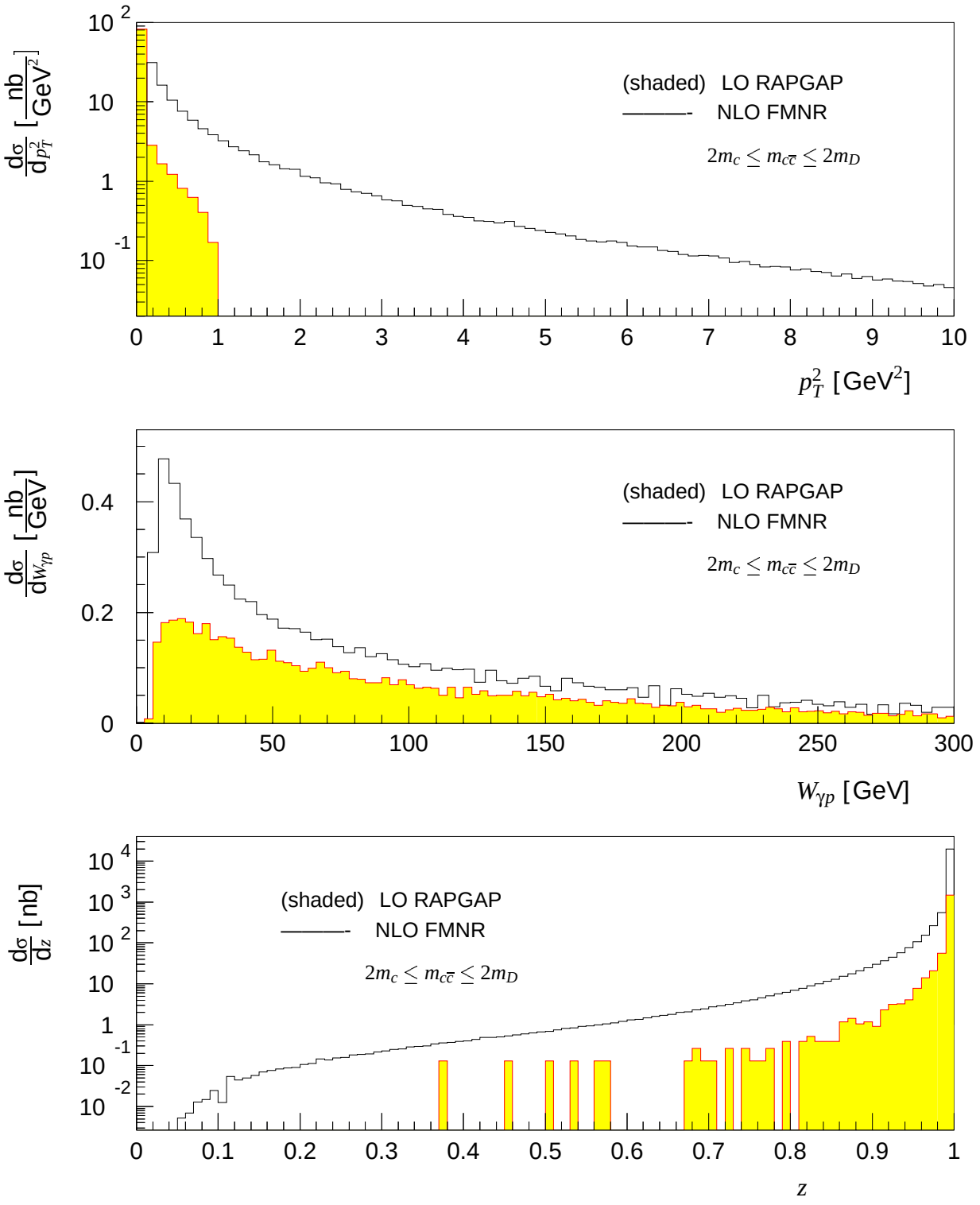

Figure 4.5: Pointlike component of the ep cross sections in the color evaporation model as a function of p_T^2, $W_{\gamma p}$ and z calculated in leading order by RAPGAP (shaded) and in next to leading order by the FMNR program (solid line). Both distributions represent the color evaporation model. A cut on the invariant mass of $2m_c \leq m_{c\bar{c}} \leq 2m_D$ was made. For details see text.

4.2.2 Comparison of the Predictions of the FMNR Program and Halzen et al.

For the comparison of the results calculated in this analysis and the published results by Halzen et al. two checks were made. At first the total cross sections for a specific photon energy were calculated and compared with predictions from the publication [Ha3]. The predictions of the color evaporation model were calculated with the FMNR program as described in chapter 4.1.2. The cross section after the integration over the invariant mass of the $c\overline{c}$ pair is obtained by integrating over the z distribution with the mass cut applied. The normalization follows the description in section 4.1.
The results are seen in figure 4.6. The four black points show the cross sections calculated with the FMNR program. The lines are the predictions of the color evaporation model published in [Ha3] for two different parton density functions. The four black points are in good agreement with the predictions of Halzen et al.

A comparison of the z distributions of the predictions by Halzen et al. published in [Ha6]

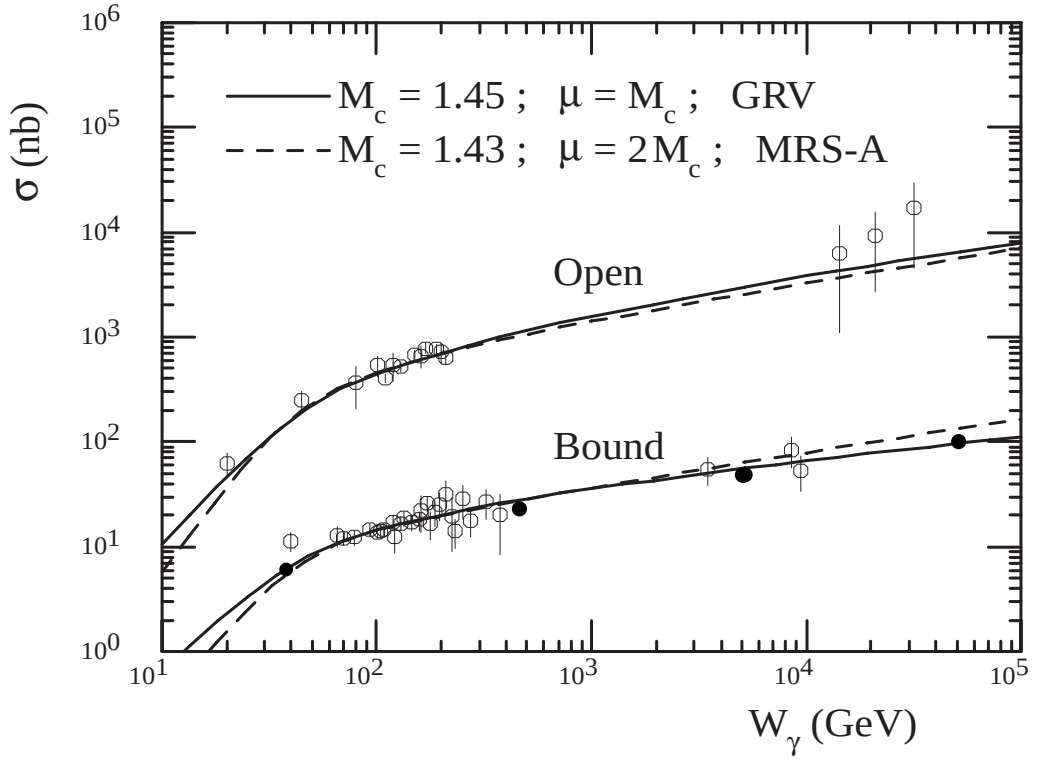

Figure 4.6: Comparison of the γp cross section for photoproduction for fixed target experiments of the published color evaporation model prediction (line) and the color evaporation model cross sections calculated by the FMNR program (black points). $MRS(A')$ was used as PDF. W_γ is the photon energy.

with the prediction by the FMNR program is made in figure 4.7. Since FMNR is only able to calculate γp cross sections for monochromatic photons the comparison of the published paper

is made with the photon-proton cross section for a center of mass energy of $W_{\gamma p} = 120\,\mathrm{GeV}$. In addition a charm mass of $m_c = 1.4\,\mathrm{GeV}$ is taken instead of $m_c = 1.3\,\mathrm{GeV}$ as in the publication. Since in figure 4.7 a) the distributions for the correction factor $Q_0 = 2m_c$ are describing the data best $Q_0 = 2m_c$ is chosen for the FMNR program as well [3]. The distribution calculated by the FMNR program is found to show the same effect as the published one. The high peak for $z \to 1$ as observed previously is suppressed. When using different $W_{\gamma p}$ energies the shape of the z distribution changes only slightly. The z distribution calculated by the FMNR program for $W_{\gamma p} = 120\,\mathrm{GeV}$ and normalized to the color evaporation model was observed to be about one order of magnitude below the results published by Halzen et al. Therefore a factor of 7 was applied to the distribution in order to compare the two distributions. This factor was investigated but not understood.

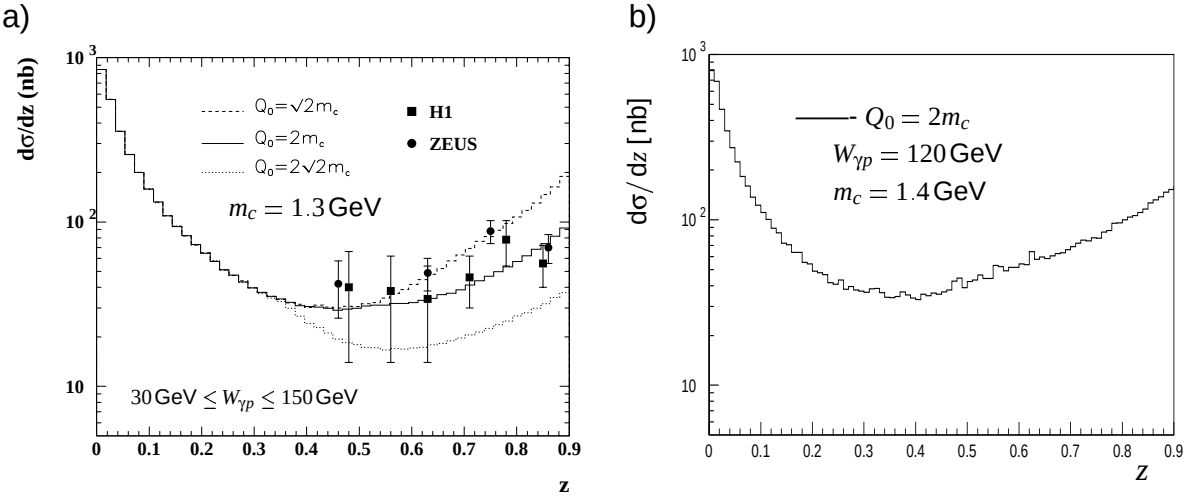

Figure 4.7: γp cross sections as a function of z, a) as published in [Ha6] and b) as calculated with the FMNR program. For b) the correction factor $Q_0 = 2m_c$ was chosen. A factor of 7 was applied to b). A cut of $p_T^2 \geq 1\,\mathrm{GeV}$ is made for both figures.

4.2.3 Comparison of EPJPSI and the FMNR Predictions

In this section comparisons between the next to leading order predictions of the color evaporation model (calculated by the FMNR program) and the leading order color singlet model Monte-Carlo generator EPJPSI are made. A comparison with the data follows in section 4.3.
As described in section 3.1.1 it is possible to include some hadronic contributions in the simulations of EPJPSI, i.e. $gg \to J/\psi g$ and $gg \to J/\psi\gamma$. For the present comparison only the pointlike contributions were selected.
The CSM requires a hard gluon to be emitted in order to form the J/ψ meson. The hard gluon carries a fraction of the photon energy away. Therefore the CSM has a strong minimum for the

[3] Furthermore whenever investigating distributions that are corrected for double counting $Q_0 = 2m_c$ is chosen for the correction factor.

cross section of inelastic J/ψ-production in the high z region, in particular for high z and high p_t. The fraction of the γp energy carried away by the gluon increases for higher p_T because the gluon has to compensate for the transverse momentum of the J/ψ meson. The Monte-Carlo generator EPJPSI is compared with the CEM as calculated with the FMNR program in order to investigate the differences between the color singlet model and the color evaporation model. The settings for the Monte-Carlo generator are chosen to be the same as the ones used for the FMNR program to ensure comparability. The cuts applied to the distributions are shown in table 4.2. The θ_μ cut is replaced by a lower cut on z in the next section.

distribution	$W_{\gamma p}$ cut	p_T^2 cut	z cut	θ_μ cut
z	$60\,\text{GeV} < W_{\gamma p} < 180\,\text{GeV}$	$p_T^2 > 1\,\text{GeV}$	-	-
$W_{\gamma p}$	-	$p_{T_{J/\psi}}^2 > 1\,\text{GeV}$	$z < 0.9$	-
$p_{T_{J/\psi}}$	$60\,\text{GeV} < W_{\gamma p} < 180\,\text{GeV}$	-	$z < 0.9$	$20^\circ \leq \theta_\mu \leq 160^\circ$

Table 4.2: Cuts applied to the distributions in figures 4.8. In addition a cut of $Q^2 \leq 1\,\text{GeV}$ was applied.

EPJPSI is compared with the predictions of the color evaporation model with and without the correction factor for double counting (see equation 2.27). The results are shown in figure 4.8. The FMNR cross sections are found to be about one order of magnitude lower than the EPJPSI cross sections. For better comparability a factor of 9 was applied to the distributions calculated by the FMNR program. A factor 7 was already observed in the previous section.
The distributions for the three variables p_T^2, $W_{\gamma p}$ and z are shown in figure 4.8. For each variable three different distributions are plotted. The EPJPSI cross section (dotted line) and the FMNR cross sections with (dashed line) and without (solid line) the correction factor.
In figure 4.8 a) the p_T^2 distributions have a strong peak for low p_T^2. The uncorrected FMNR distribution has a similar slope as the EPJPSI distribution while the corrected FMNR distribution shows a flatter slope. For the z distribution in figure 4.8 c) the slope of the corrected FMNR distribution is flatter than the uncorrected distribution again but this time very similar to the EPJPSI prediction. The EPJPSI z distribution shows in contrast to the FMNR distributions no peak for high z. This is due to the hard gluon being emitted as described above and the relativistic corrections being excluded. For $W_{\gamma p}$ the EPJPSI distribution and the corrected distribution have a similar shape although the corrected cross section is slightly higher than the EPJPSI cross section. The uncorrected FMNR distribution has a more pronounced peak at low $W_{\gamma p}$. The FMNR predictions with the correction factor therefore seem to fit to the $W_{\gamma p}$ and z distributions of EPJPSI except for the high z region where the cross section for the color singlet model is expected to decrease rapidly due to the emitted hard gluon that limits the phase space. For p_T^2 the corrected FMNR distribution is too flat to describe the EPJPSI distribution. The FMNR distributions that are not corrected for double counting instead have a high maximum for high z and a narrower but higher peak than the EPJPSI distribution in the $W_{\gamma p}$ distribution at $W_{\gamma p} \approx 20\,\text{GeV}$.
The comparison of EPJPSI with FMNR seems to favor the corrected predictions, though the p_T^2 distribution with the correction factor is too flat to describe the EPJPSI distribution. For a more reliable statement the distributions have to be compared to the data.

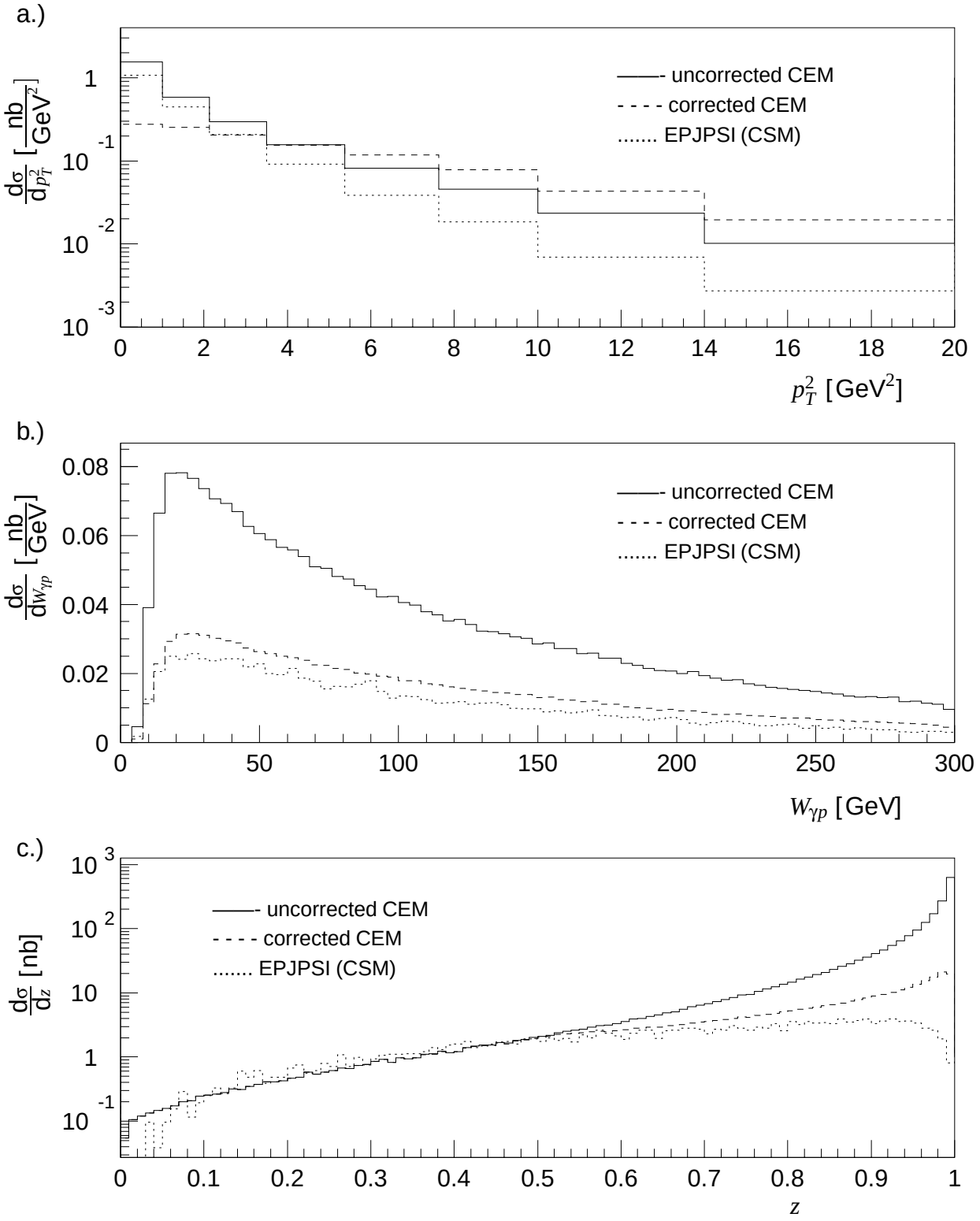

Figure 4.8: *ep* cross sections of the pointlike component of the color singlet model Monte-Carlo generator EPJPSI (dotted line) compared with the cross sections of the FMNR program. The solid line represents the cross section for the FMNR program without the correction factor and the dashed line with the correction factor as described in equation 2.27. The cuts are described in table 4.2. The distributions of the FMNR program were multiplied by a factor 9 to match them to EPJPSI.

4.2.4 Comparison of the Berger-Jones Cross Section and the Cross Section of the FMNR Program

In this section a comparison of the cross section as calculated in [BeJ] (see equation 2.14) and for the pointlike component of EPJPSI and the FMNR program is made. The differential cross sections for the $log(x)$ distribution (introduced in section 2.3.1) are shown in figure 4.9. The logarithm of x is plotted on the x-axis. x is defined as $x = \frac{s'}{\hat{s}}$ where s' is the photon gluon energy. Since for the FMNR program s' was not available x was approximated for the FMNR program by equation 2.15. The settings and cuts applied to the distributions are shown in table 4.3.

	$W_{\gamma p}$	$m_{J/\psi}, m_c$	PDF	z
Berger Jones	$W_{\gamma p} = 100\,\text{GeV}$	$m_{J/\psi} = 3.1\,\text{GeV}$	$G(x) = \frac{3(1-x)^5}{x}$	-
Berger Jones	$W_{\gamma p} = 100\,\text{GeV}$	$m_{J/\psi} = 3.1\,\text{GeV}$	$MRS(A')$	-
EPJPSI	$90 \leq W_{\gamma p} \leq 100\,\text{GeV}$	$m_{J/\psi} = 3.1\,\text{GeV}$	$MRS(A')$	$z \leq 0.9$
FMNR	$W_{\gamma p} = 100\,\text{GeV}$	$m_c = 1.5\,\text{GeV}$	$MRS(A')$	$z \leq 0.9$

Table 4.3: Cuts and settings applied to the distributions in figures 4.9.

The four distributions in figure 4.9 are arbitrarily normalized. The solid and the dotted line show cross sections predicted by the Berger-Jones equation 2.14. The dotted line is calculated with the simplified gluon density given in equation 2.17 and the solid line with the gluon density parameterization of the PDF set $MRS(A')$ (equation 2.18). The two predictions are calculated for $W_{\gamma p} = 100\,\text{GeV}$. Both distributions show a similar behavior, they start at approximately $log(x) = -3.04$ and have a maximum for $log(x) \approx -2.8$. The dotted line is a bit wider than the solid line. This is explained by the different gluon densities used.
The shaded area is the EPJPSI cross section. It is simulated for a photon proton energy range of $90\,\text{GeV} \leq W_{\gamma p} \leq 100\,\text{GeV}$. The EPJPSI distribution starts at $log(x) = -3$. It appears to have the maximum slightly shifted to higher x but is in good agreement with the Berger-Jones distribution with the same PDF set $MRS(A')$.
The distribution of the FMNR program is represented by the dashed line. It shows a slower increase at $log(x) \approx -3$ than the other distributions. The maximum is shifted towards higher x and is at $log(x) \approx -2.5$. The FMNR distribution also shows a slower decrease for higher x. It is in general flatter than the other distributions and shifted towards higher x. The different behavior of the distribution calculated with the FMNR program should be investigated further, this will not be done here. This distribution is the only distribution containing full next to leading order contributions.

4.3 Comparison of the FMNR predictions with Data

The color evaporation model will now be compared with data measured by the H1 collaboration in the years of 1995-97. The data selection is discussed in detail in [Kru00].

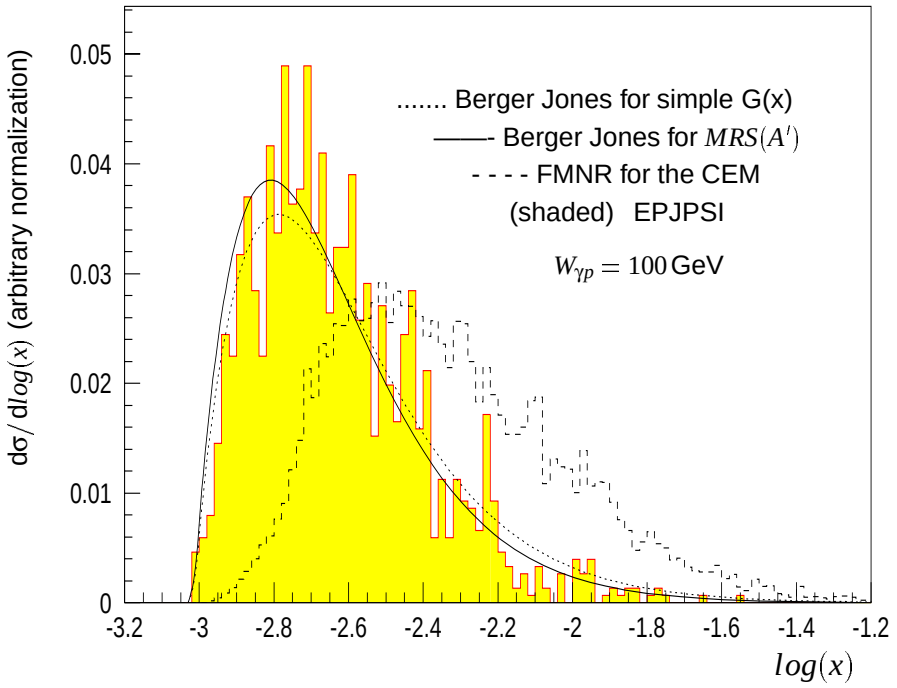

Figure 4.9: γp cross sections as a function of $log(x)$ with arbitrary normalization. The dotted line is calculated from equation 2.14 with the simplified gluon density of equation 2.17 and the solid line is calculated with the gluon density from the PDF set $MRS(A')$. The shaded area is the EPJPSI cross section. The dashed line shows the color evaporation model predictions calculated with the FMNR program with the factor for double counting.

4.3.1 Comparison of Differential Cross Sections

In this section differential ep cross sections for $W_{\gamma p}$, p_T^2, and z distributions obtained with the FMNR program are compared with the data. The data set is corrected for trigger efficiencies and detector cuts. The kinematical cuts are similar to the ones in the previous section. Instead of the cut on θ_μ which is applied to the data a cut $z \geq 0.3$ was made (see table 4.4). FMNR predictions with and without the correction factor for double counting as described in section 2.3.3 are compared with the data in figure 4.10.

distribution	$W_{\gamma p}$ cut	p_T^2 cut	z cut
z	$60\,\text{GeV} < W_{\gamma p} < 180\,\text{GeV}$	$p_T^2 > 1\,\text{GeV}$	-
$W_{\gamma p}$	-	$p_{T_{J/\psi}}^2 > 1\,\text{GeV}$	$0.3 \leq z \leq 0.9$
$p_{T_{J/\psi}}$	$60\,\text{GeV} < W_{\gamma p} < 180\,\text{GeV}$	-	$0.3 \leq z \leq 0.9$

Table 4.4: Cuts applied to the FMNR distributions in figures 4.10. In addition a cut of $Q^2 \leq 1\,\text{GeV}$ was applied.

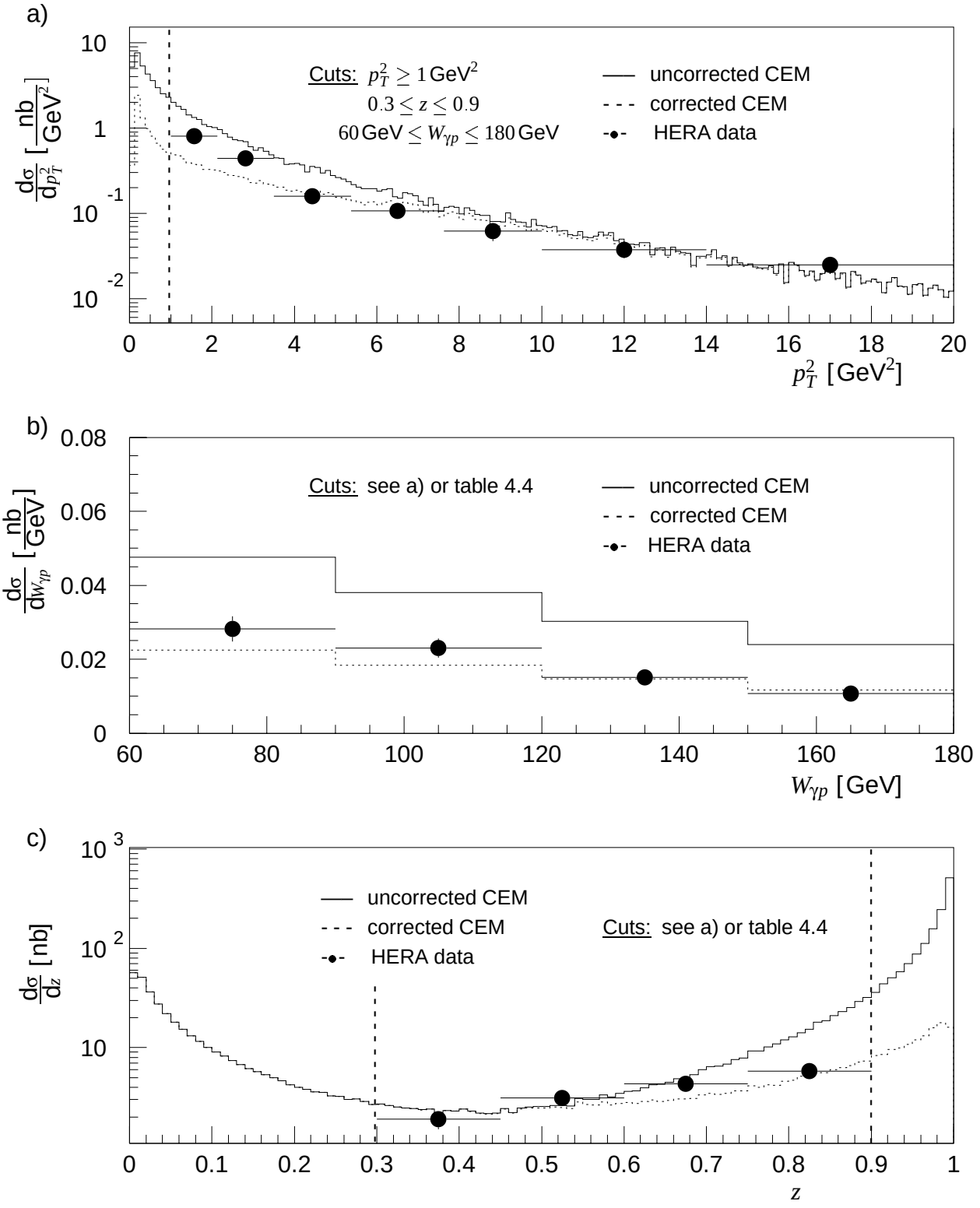

Figure 4.10: Differential ep cross sections as a functions of a) p_T^2, b) $W_{\gamma p}$ and c) z for the color evaporation model predictions with (dotted line) and without (solid line) double counting factor applied. The dots are data from [Kru00]. $MRS(A')$ was used as proton PDF and the factors $\rho_{J/\psi} = 0.43$ and $\frac{1}{9}$ were applied to normalize the FMNR distributions to the color evaporation model. The cuts are indicated in the figure, they are applied to the FMNR distributions and the data. The cuts $p_T^2 \geq 1\,\mathrm{GeV}^2$ and $0.3 \leq z \leq 0.9$ are not applied to the p_T^2 and z distribution respectively. The cuts are indicated by the dashed lines. A factor of 9 was applied to all distributions of the FMNR program.

The FMNR distributions were again integrated and normalized to represent the color evaporation model as described in section 4.1.2. As seen in the previous section the predictions of the FMNR program are about one order of magnitude too low, thus again a factor of 9 is applied to the distributions in order to fit the distributions to the data.
In figure 4.10 the comparisons of the FMNR distributions with the data are shown. In this figure the black points are the data and the two lines are the cross sections calculated by the FMNR program. The dotted line shows the predictions with and the solid line without the correction factor for double counting. All distributions are shown as differential ep cross sections. No data were available for $p_T^2 \leq 1\,\mathrm{GeV}$, $z \leq 0.3$ and $z \geq 0.9$. Therefore cuts were applied to exclude these regions. In addition a cut of $60\,\mathrm{GeV} \leq W_{\gamma p} \leq 180\,\mathrm{GeV}$ is made. The p_T^2 cut was not applied to the p_T^2 and the z cut was not applied to the z distribution in order to see the predicted shape calculated by the FMNR program in the excluded regions. The cuts are indicated by a dashed line.
All three p_T^2 distributions show a similar behavior. They have a peak at low p_T^2 and decrease for higher p_T^2. The uncorrected distribution calculated by the FMNR program (solid line) has the steepest slope, the corrected distribution has the flattest slope. The corrected cross section is nearly identical to the uncorrected cross section for $p_T^2 \geq 8\,\mathrm{GeV}^2$. For lower p_T^2 the dotted line is flatter and describes the data well for $p_T^2 \geq 3.5\,\mathrm{GeV}^2$. Below $3.5\,\mathrm{GeV}^2$ the prediction is too low. The solid line is too steep to describe the data. The tendency to a too flat slope for the corrected distribution for the low p_T^2 region was already observed in [Ha6], see also figure 2.10 a).
For the $W_{\gamma p}$ distributions a similar behavior is observed. The cross sections decrease for high $W_{\gamma p}$ and the uncorrected distribution has the steepest slope. The corrected cross section has the flattest slope. Again the dotted line is in fair agreement with the data. The solid line is about a factor of 2 higher than the data.
For all distributions both the hadronic and pointlike components are included in the calculations. This can be seen in the z distribution. The cross sections calculated by the FMNR program show a peak for low z from the hadronic contributions and a peak for high z from the pointlike contributions. For $z \leq 0.5$ the corrected and the uncorrected distributions are identical. For higher z the uncorrected cross section shows a steep slope while the corrected one is flatter. The data only cover the region of $0.3 \leq z \leq 0.9$ as already mentioned above. The data show a good agreement with the dotted line. This is expected since the correction factor was introduced to match the z distribution to the data.
The corrected FMNR cross sections are in a good agreement with the data. The uncorrected cross sections show a too steep behavior for all three distributions.

4.3.2 Comparison of Double Differential Distributions

Recent results of the p_T^2 distributions in different z bins will be published in [Kru00]. These results show that neither the color octet nor the color singlet model can describe the z dependence of the p_T^2 distribution. In this section the data are compared with the EPJPSI distributions and with the corrected and uncorrected FMNR distributions.
The data used for this comparison are not corrected for the kinematical cuts. In order to compare these raw data with the EPJPSI predictions detector cuts were included in the calculations. The cuts applied are:

- $60\,\text{GeV} < W_{\gamma p} < 180\,\text{GeV}$
- $p_{T_\mu} > 1.1\,\text{GeV}$, with p_{T_μ} being the momentum of the decay muons from the J/ψ.
- $20^\circ < \theta_\mu < 160^\circ$ since the muon-detection includes the central tracking detectors.

The latter cuts cannot be applied for the FMNR distributions since it is only calculating open $c\bar{c}$-pairs (see chapters 2.3.3 and 3.2). There are no decay products of the J/ψ-Meson available for FMNR calculations. The muon properties are assumed to correlate to the properties of the two single c quarks in the FMNR program (see section 4.1.2). Therefore the same angular cut is applied to the single charm quarks. For the p_{T_μ} cut the same assumption was made. A cut of $p_{T_c} > 1.1\,\text{GeV}$ was applied instead. The p_{T_μ} and θ_μ cut reflect the selection cuts applied to the muons in the experiment.
The data are not presented as cross sections but as $\frac{1}{N}\frac{dN}{dp_T^2}$ in order to allow the comparison of the shapes of the distributions. N is the total number of events in a given distribution. EPJPSI is normalized in a similar way. For the FMNR program the distributions of $\frac{1}{\sigma}\frac{d\sigma}{dp_T^2}$ is shown since FMNR calculates cross sections and not events. All distributions are therefore normalized to 1. The normalization factors are presented in table 4.5. The factor 9 as used for the FMNR program in previous sections is not applied here. The table shows similar normalization factors for each z bin except for the FMNR distribution without the correction factor for high z. The latter increases rapidly for high z as expected due to the strong maximum for $z \to 1$.

Figure 4.12	Data N	EPJPSI N	FMNR uncorr. σ [nb]	FMNR corr. σ [nb]
a)	25.81	1172.0	0.02098	0.01959
b)	31.92	1016.0	0.02324	0.01106
c)	35.07	1359.0	0.07809	0.01529
d)	27.39	863.4	0.4254	0.01541

Table 4.5: Normalization factors for the double differential distributions of FMNR,EPJPSI and the data. The factor of 9 that was applied to the FMNR program in previous sections was not applied here.

The p_T^2 distributions in the four different z bins in figure 4.11 are shown for the data (black points) and for EPJPSI (shaded histogram). The data have a nearly constant p_T^2 slope for the four z regions. The slope of EPJPSI is getting steeper for higher z regions. The highest p_T^2 data point is not described in any z region. EPJPSI can not describe the p_T^2 distribution of the data, especially not for high z. The suppression of high z and high p_T^2 cross sections in the color singlet model is already discussed in section 4.2.3.
In figure 4.12 the p_T^2 distributions calculated by the FMNR program are compared with the data. The solid line represents the color evaporation model without the double counting correction factor applied, the dotted curve shows the cross sections with the correction factor applied. The uncorrected distributions have a nearly constant slope for the four z regions and are in agreement with the data. The corrected distributions show a fundamental change in their shape when proceeding from the low z bins to the higher z bins. The low p_T^2 region is more and more

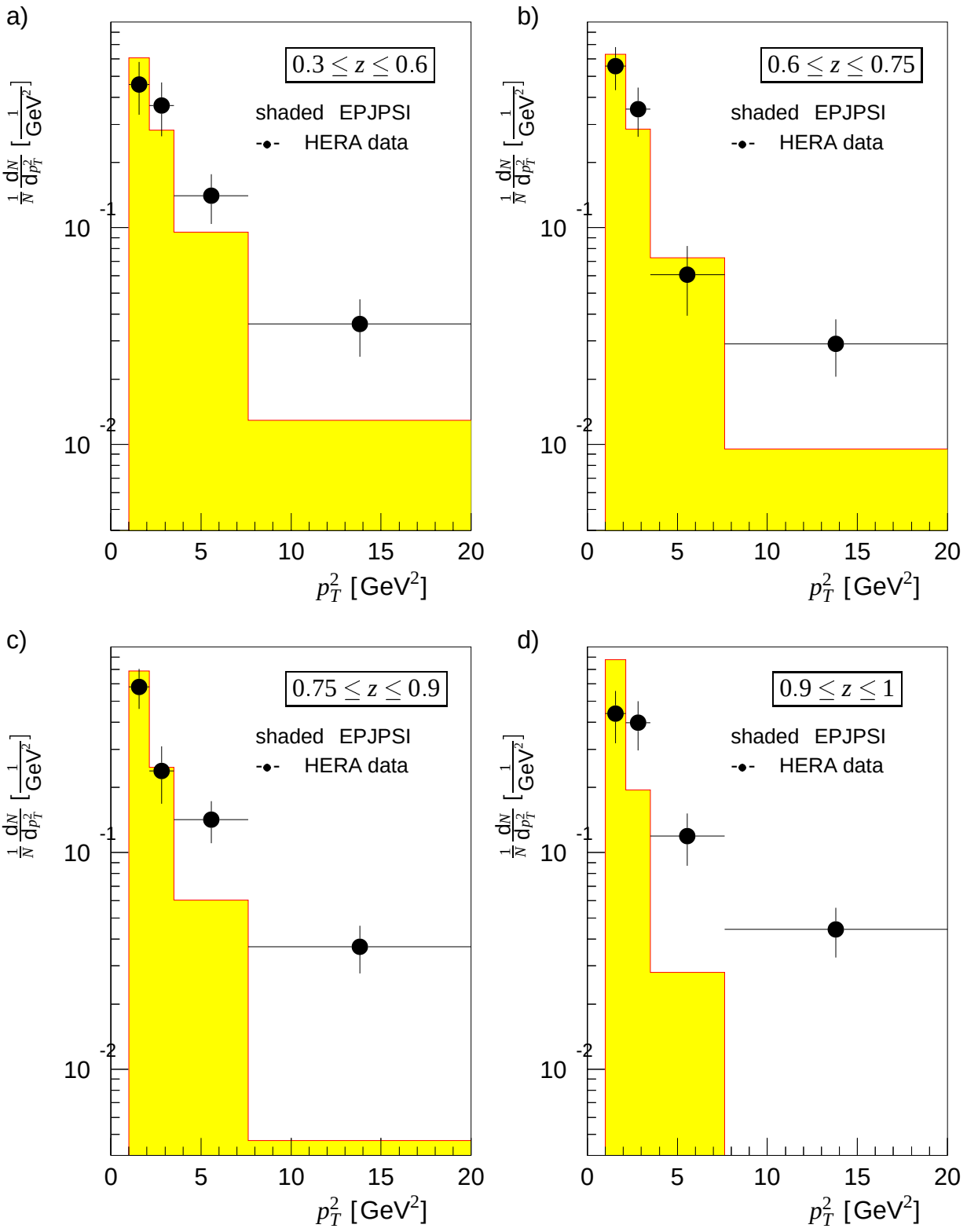

Figure 4.11: p_T^2 distributions for four different z bins. The distributions are normalized to 1. The normalization factors N for data and EPJPSI are listed in table 4.5. The cuts applied to the four distributions are described in the text.

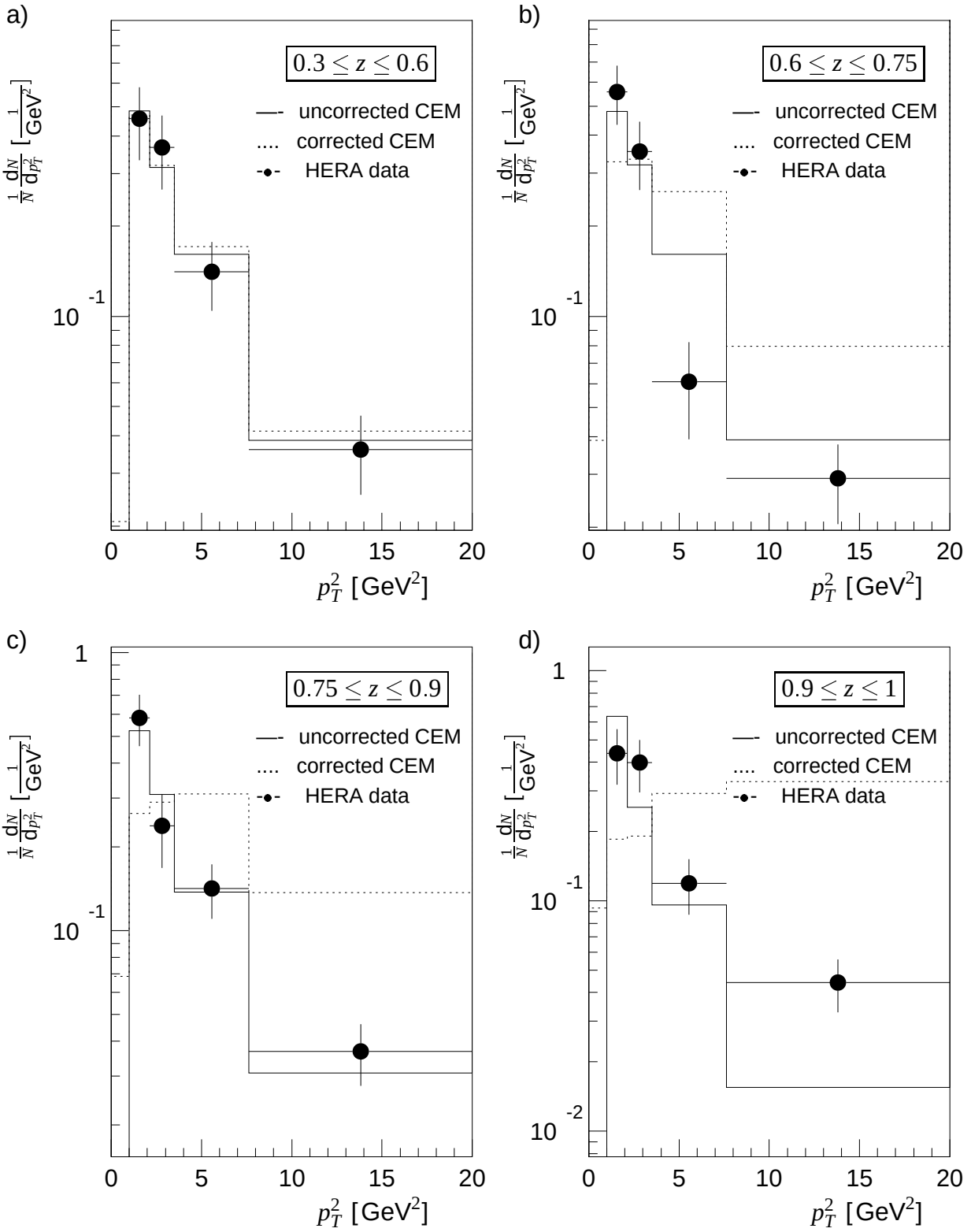

Figure 4.12: p_T^2 distributions for four different z bins. The distributions are normalized to 1. The normalization factors are listed in table 4.5. The cuts applied to the four distributions are described in the text.

suppressed the closer the z region approaches 1. In the highest z region the slope of the corrected distribution even has the opposite sign than the slope of the data. Since the correction factor increases exponentially for high z and low p_T^2 this behavior was to be expected. The FMNR distributions after the correction for double counting cannot describe the data.

4.4 Conclusions from the Comparisons

For all distributions of the color evaporation model as calculated with the FMNR program a factor of 9 had to be applied in order to achieve agreement with the cross sections of EPJPSI or the data. Since the distributions published by Frixione et al. was reproduced fairly well the factor cannot result from the program. In addition the publications by Halzen et al. fit the data without the factor applied. The factor therefore should result from the integration or normalization. The origin of this factor is not understood.
In the comparison of FMNR and EPJPSI the distributions of FMNR with the phenomenological correction factor which suppresses high z and low p_T^2 appear to be in a better agreement with the predictions of EPJPSI for the z and $W_{\gamma p}$ distributions. Nevertheless the uncorrected p_T^2 distribution as calculated by the FMNR program describes the p_T^2 distribution of EPJPSI better. The comparisons with the data show a good agreement with the corrected cross sections calculated by the FMNR program for all distributions. The correction factor was introduced by Halzen et al. in order to describe the z and the p_T^2 distributions. The uncorrected z distribution shows the same maximum for high z as the distributions of the leading order color octet model. The uncorrected p_T^2 distribution shows a too steep slope.
For the p_T^2 distributions in four z regions only the shapes were compared. The distributions of EPJPSI show a too steep slope. EPJPSI cannot describe the highest p_T^2 bin for any z region.
The distributions of the FMNR program were normalized to $\frac{1}{\sigma}\frac{\mathrm{d}\sigma}{\mathrm{d}p_T^2}$ for the double differential distributions. The uncorrected distributions of FMNR are in good agreement with the data for the double differential distributions. The corrected distributions of FMNR show a somewhat strange behavior. The distribution is still in good agreement with the data for the lowest z region but completely different for the highest z region where the correction factor has the strongest impact. The distributions suggest that the correction factor introduced to suppress double counting of events should be modified. The correction factor should suppress the strong maximum for high z and low p_T^2 but it should not change the shape for the double differential distributions.
The FMNR distributions of p_T^2, $W_{\gamma p}$ and z with the correction factor for double counting are in good agreement with the data. A factor of 9 had to be applied to the FMNR distributions. The double differential distributions calculated by the FMNR program without the correction factor however are in better agreement with the data than the corrected distributions or the EPJPSI distributions.

Summary

In this thesis the color evaporation model (CEM) for inelastic J/ψ production was investigated. In the color evaporation model the production of an "open" $c\bar{c}$ pair is calculated and the color of the produced $c\bar{c}$ pair is assumed to be 'bleached out' (evaporate) by multiple soft gluon interactions. The cross section for J/ψ production in the color evaporation model is calculated by integrating the $c\bar{c}$ cross section over a mass interval of $[2m_c, 2m_D]$ and applying factors corresponding to a statistical treatment of color.
The FMNR program, a program for next to leading order open $c\bar{c}$ pair production, is used to calculate the color evaporation model predictions. The distributions are calculated by limiting the invariant mass of the open $c\bar{c}$ pair to the above mass interval and applying a normalization factor suggested by Halzen et al. In the FMNR program the pointlike and hadronic contributions can be calculated separately. Both components have to be added in order to yield results that can be compared with the data in the whole kinematic region.
The distributions of the color evaporation model were calculated with and without a phenomenological correction factor introduced by Halzen et al. The correction factor suppresses double counting of events due to the ambiguity of some next to leading order contributions which are already accounted for by leading order diagrams. This correction factor mainly suppresses the high z and low p_T^2 regions.
The next to leading order color evaporation model predictions were compared with a Monte-Carlo generator for the color singlet model and data taken at the H1 detector at HERA.
The Monte-Carlo generator EPJPSI was chosen to simulate J/ψ production in the color singlet model. For the comparison with EPJPSI a normalization factor of 9 had to be introduced in order to obtain agreement of the color evaporation model cross sections with the color singlet ones. The comparison of the color singlet model and the color evaporation model shows an acceptable agreement in the z and $W_{\gamma p}$ distributions for the CEM with the high z correction factor. The p_T^2 distribution of the color singlet model is better described by the uncorrected CEM distribution.
The data used in this analysis were taken with the H1 detector in the period between 1995 and 1997. The analysis and selection of the data was performed by [Kru00]. In order to describe the data a factor of 9 had to be applied to the CEM cross sections. This factor was investigated but not understood.
The z distribution of the color evaporation model with the correction factor for double counting is in agreement with the data. For high z the uncorrected cross section shows the same peaking at $z \to 1$ as the color octet model. The $W_{\gamma p}$ distribution of the data can be described by the corrected $W_{\gamma p}$ distribution calculated by the FMNR program as well but the uncorrected $W_{\gamma p}$ distribution shows a too steep slope. In the present analysis a larger range of p_T^2 than in

previous publications of the color evaporation model by Halzen et al. is investigated. The corrected p_T^2 distribution is in a fair agreement with the data while the uncorrected one is again too steep.
In addition double differential distributions of p_T^2 in different z bins were compared to the data. Here only the shape of the distributions was compared. The distributions show a very good agreement of the shape for the uncorrected cross sections calculated by the FMNR program and the data. The corrected FMNR predictions and the predictions of EPJPSI cannot describe the shape of the data particularly for the higher z bins. The double differential distributions could not be described by any Monte-Carlo generator (see [Kru00]).For the FMNR distributions corrected for double counting the shape changes dramatically for the high z bins, the slope of p_T^2 has the opposite sign of the slope of the data for $0.9 \leq z \leq 1$. This effect results from the exponential increase of the correction factor for high z. This implies that the correction factor should be changed in order to describe the double differential distributions as well. Since the uncorrected distributions describe the shape of p_T^2 in the four z bins it should be possible to change the present factor accordingly.
With these results the color evaporation model should not be excluded for the description of the data. For future analyses an improved correction factor for the color evaporation model should be developed. The new factor has to describe the z distribution of the data while decreasing the impact on the shape of the double differential distributions. In addition an analysis with the color evaporation model for the low z region, where hadronic contributions play a major role should be pursued.

Appendix A

The Complete Settings

In this chapter the steering card parameters are given for the Monte-Carlo generators EPJPSI and RAPGAP and for the FMNR program. The parameters that are not listed in the tables were set to the default values. For FMNR only the steering card for the comparison with the data and the Monte-Carlo generators are given. At last a list of the scaling factors used in this analysis is given.

A.1 For EPJPSI

In table A.1 the parameters for the EPJPSI Monte-Carlo generator are given. For further details about the parameters or a list of the default values see [Jun1].

A.2 For RAPGAP

In table A.2 the parameters for the RAPGAP Monte-Carlo generator are given. For further details about the parameters or a list of the default values see [Jun1].

A.3 For the FMNR program

A.3.1 For the Pointlike Component of the FMNR program

In table A.3 the parameters for the pointlike component of FMNR are given. This is the complete steering card. The energy given is half the center of mass energy of the collision.

RAPGAP parameter	value	explanation
'PPIN'	820.	proton beam energy [GeV]
'PLEP'	-27.5	electron beam energy [GeV]
'LEPI'	11	LUND code
'NFRA'	1	fragmentation
'IRAS'	1	fixed/running $alpha_s$
'IWPS'	1	uncorr./corr. width of J/ψ
'NSTR'	1003039	struc. fct. for proton $MRS(A')$
'NSTG'	3005006	struc. fct. for photon $GRV-HO$ PDFLIB: $10^6 \cdot NPTYPE + 1000 \cdot NGROUP + NSET$ is used as coding scheme
'IQ2S'	3	struc. fct. for photon $GRV-HO$: $q^2 = m^2 + pt^2$
'IPRO'	1	γ gluon $\rightarrow J/\psi$ gluon
'EPSM'	0	epsilon/m (no rel. corr.)
'QMIN'	0.	Q^2_{min} of electron
'QMAX'	1.0	Q^2_{max} of electron [GeV]
'MDME'	1	$J/\psi \rightarrow \mu\bar{\mu}$, the only decay possibility

Table A.1: Steering parameters for EPJPSI. Values not listed are set to the default value. A description for each variable is found in the right column. For more details see [Jun1].

A.3.2 For the Hadronic Component of the FMNR program

In table A.4 the parameters for the pointlike component of FMNR are given. This is the complete steering card. The energy given is half the center of mass energy of the collision. This is only one of the twenty photon energies used. For the calculation of the other energies only the beam energy was changed according to table A.5.

A.4 Scaling Factors

In table A.6 the scaling factors used in the different programs and by Halzen et al. are shown.

RAPGAP parameter	value	explanation
'PPIN'	820.	proton beam energy [GeV]
'PLEP'	-27.5	electron beam energy [GeV]
'LEPI'	-11	LUND code
'NFRA'	0	no fragmentation
'IRAS'	1	fixed/running α_s
'IRAM'	1	fixed/running $\alpha_E M$
'ITIM'	0	=0 no shower of time like parton
'IQ2S'	3	scale of struc. fct. α_s: $q^2 = m^2 + pt^2$
'IPRO'	14	process for direct QQ: $e$gluon $\rightarrow c\bar{c}$ (full ME)
'KT1 '	0.	intrinsic k_t for photon
'KT2 '	0.	intrinsic k_t for proton
'INPR'	1005006	proton structure function GRV
'INGA'	3005002	photon structure function GRV L $10^6 \cdot NPTYPE + 1000 \cdot NGROUP + NSET$ is used as coding scheme
'ISET'	3	ISET of SaSgam
'IP2 '	0	IP2 of SaSgam
'OMEG'	0.01	suppression factor for virtual γ
'NFLA'	3	number of flavors used
'IDIF'	0	no mixing of DIS, diffractive and pion exchange
'IFUL'	1	quark parton model with $O(\alpha_s)$ matrix elements
'IGRI'	0	QCD weights calc per event
'IVME'	0	no special selection on vectormeson
'IINT'	0	BASES/SPRING Integration procedure
'NCAL'	5000	number of calls per iteration for bases
'QMIN'	0.	Q^2_{min} of electron
'QMAX'	1.	Q^2_{max} of electron [GeV]
'PMAS'	1.40	mass of charm quark [GeV]

Table A.2: Steering parameters for RAPGAP. Values not listed are set to the default values. A description for each variable is found in the right column. For more details see [Jun2].

'test2'	identification string
1	1 for restart files
'fmnrout2'	prefix for files
$1.5000D+02$ $0.1400D+01$ $0.2000D+01$ $0.2000D+01$ $0.1000D+01$	energy, mass, scale factor for photon, hadron and renormalization
$-.1000D+01$ $-.1000D+01$ $-.1000D+01$ $-.1000D+01$ $-.1000D+01$	for only one collision
3	number of light flavors
0	default charge
1	hadron types (proton)
339	PDF set for nucleon
0	$\Lambda_5(\text{GeV}) = 0$ for default or $0.1300D+00$
'MS'	scheme for Photon (DI oder MS)
1 0 0	double single total
1	0=monochromatic photon beam, 1=userfile for photon distribution (WW)
0	1=gg,2=qq,3=qg,0=all,-1 excl. gg, etc.
-5000 -10000	number of iterations
1 1	0 to exclude,1 for new run, 2 to restart
1000 1000	number of calls for vegas, < 0 for default

Table A.3: Steering card for the pointlike component of FMNR for electron proton collision with a center of mass energy of 300 GeV and a charm mass of 1.4 GeV. The energy given is half the center of mass energy. The PDF set for the proton is as given in the publication [PDF].

'testhad'	identification string
1	1 for restart files
'final-w65'	prefix for files
$0.32389D+02$ $0.1400D+01$ $0.2000D+01$ $0.2000D+01$ $0.1000D+01$	energy, mass, scale factor for photon, hadron and renormalization
$-.1000D+01$ $-.1000D+01$ $-.1000D+01$ $-.1000D+01$ $-.1000D+01$	for only one collision
3	number of light flavors
4 1	hadron types (photon, proton)
71	PDF set for nucleon
43	PDF set photon, beam1
0.152	$\Lambda_5(\mathrm{GeV}) < 0$ for default
1 0 0	double single total
0	1=gg,2=qq,3=qg,0=all,-1 excl. gg, etc.
-5000 -10000	number of iterations for single inc
1 1	0 to exclude,1 for new run, 2 to restart
1000 1000	number of calls for vegas, < 0 for defaults

Table A.4: Steering card for the hadronic component of FMNR for photon proton collision with a center of mass energy of 64.778 GeV and a charm mass of 1.4 GeV. The PDF sets are defined by Frixione et al. and are included in the FMNR program. 71 is the $MRS(A')$ proton PDF and 43 is the $GRV-HO$ photon PDF.

$W_{\gamma p}$ center in GeV	64.778	74.804	84.822	94.838	104.848	114.857
$W_{\gamma p}$ center in GeV	124.865	134.871	144.876	154.880	164.884	174.888

Table A.5: The center of the $W_{\gamma p}$-bins for the 10 GeV $W_{\gamma p}$-bins between 60 GeV and 260 GeV used.

program	scale factor Q^2_{scale}
FMNR	$Q^2_{scale} = \frac{p^2_{T_c}+p^2_{T_{\overline{c}}}}{2} + m_c^2$
RAPGAP	$Q^2_{scale} = p_T^2 + m_c^2$
EPJPSI	$Q^2_{scale} = p_T^2 + m_c^2$
Halzen et al.	$Q^2_{scale} = s''$ with $s'' = x_A x_B W_{\gamma p}$ for the subprocess $AB \to c\overline{c}$

Table A.6: Scale factors used in this analysis.

List of Figures

1.1 The storage ring HERA (right) and its preaccelerators (left) at DESY. 4

1.2 A schematic overview of the H1 detector. 5

2.1 A generic diagram for ep scattering. X designates any hadronic final state, the variables are described in the text. 7

2.2 J/ψ-production via boson gluon fusion in the color singlet model. 9

2.3 Diagram for the production of a quark antiquark pair via boson-gluon fusion. . 10

2.4 $O(\alpha_{em}\alpha_s^2)$ processes contributing to a) pointlike and b) hadronic charmonium photoproduction. $\hat{t}$ is the momentum fraction transfered from the incoming parton (gluon, quark) to the interacting gluon (parton). 10

2.5 Graph for the production of a J/ψ-meson via photon-gluon-fusion: a) in the Color Singlet Model by emitting a hard perturbative gluon, b) in the Color Octet Model by forming a $c\overline{c}$ pair in the color octet state and emitting a soft (nonperturbative) gluon or a photon. 14

2.6 $\mathrm{d}\sigma/\mathrm{d}z$ world data 1992 for inelastic J/ψ production [EMC1]. The dash-dotted curve is the prediction of the color singlet model [BeJ]. The dashed curve from [DuO] is a calculation in leading order of the color evaporation model. The z dependence of $\mathrm{d}\sigma^2/\mathrm{d}z\,\mathrm{d}p_T^2$ at $p_T^2 = 1\,\mathrm{GeV}^2$ is plotted. Both curves are arbitrarily normalized. 14

2.7 Mechanism for the production of rapidity gaps in deep inelastic scattering in a $3 \times \overline{3}$ color state, one color singlet state and eight color octet states. 16

2.8 Hadroproduction data [Bam] and the cross sections of the color evaporation model at NLO as a function of the photon proton center of mass energy $W_{\gamma p}$ (figure from [Ha3]). 17

2.9 H1 and ZEUS data [H1Z] and the CEM γp cross sections as a function of p_T^2 for different Q_0. Cuts of $0.4 < z < 0.9$ and $p_T^2 > 1\,\mathrm{GeV}$ were applied. The GRV structure function with $\Lambda^{(4)} = 300\,\mathrm{MeV}$, renormalization scale $\mu_R = m_c$ and $m_c = 1.3\,\mathrm{GeV}$ was used (figure from [Ha6]). The factorization scale is set to $s'' = x_A x_B W_{\gamma p}^2$ for the subprocess $AB \to J/\psi X$. 18

2.10 γp cross sections as a function of z for the color evaporation model with the correction factor described in the text. In a) the z distribution is shown for three values of the correction factor Q_0. In b) a cut of $|\hat{t}| > Q_0^2 = (2m_c)^2$ was used instead of the correction factor. The remaining parameters of both distributions are the same as in figure 2.9 (figure from [Ha6]). 18

2.11 p_T distribution for the color singlet model and the color octet model from [Kra1]. The two contributions of the COM add up to the total COM prediction. The CSM predictions are several orders of magnitude smaller than the TEVATRON data. 19

2.12 HERA data from ZEUS and H1 and the predictions according to the COM and the CSM from [KrB]. The color octet model has a too high cross section for high z. 20

2.13 Data from the CDF Collaboration [CDF1] shown with arbitrary normalization. The curves are the predictions of the CEM at tree level. The normalization is correctly predicted within a factor of 2.2 (from [Ha3]). 21

4.1 γp cross sections as a function of the transverse momentum of the charm quarks. The pointlike and hadronic contributions are separately shown, together with the sum of the two. a) displays published FMNR results (figure from [FMNR7]) and b) shows the reproduced distribution. The same settings are used for both distributions. 28

4.2 a) ep cross section as a function of the invariant mass of the $c\overline{c}$ pair. The pointlike and hadronic component as calculated by the FMNR program for $m_c = 1.3\,\text{GeV}$ (solid line) and $m_c = 1.4\,\text{GeV}$ (dashed line) are shown. For the color evaporation model only contributions from $2m_c \leq m_{c\overline{c}} \leq 2m_D = 3.74\,\text{GeV}$ are taken into account. The upper cut is indicated by the dotted line. b) The integral over the cross section for $m_c = 1.3\,\text{GeV}$ divided by the integral over the cross section for $m_c = 1.4\,\text{GeV}$ with the upper limit of the integral on the x-axis. 29

4.3 ep cross sections from the FMNR program including the pointlike and the hadronic contributions as a function of a) z and b) p_T^2 for different cuts as indicated in the legend. $MRS(A')$ was used as proton PDF and $GRV-HO$ as photon PDF. A charm mass of $m_c = 1.4\,\text{GeV}$ was used. For b) the cuts are described in a), only the dotted line corresponds to the cuts indicated. 32

4.4 ep cross sections as a function of p_T^2, $W_{\gamma p}$ and z as calculated by the FMNR program with $MRS(A')$ as proton PDF, $\sqrt{s} = 300\,\text{GeV}$ and $m_c = 1.4\,\text{GeV}$. The dashed line shows the contributions of the pointlike component and the dotted line represents the hadronic contributions. The solid line is the total $c\overline{c}$ cross section. Different cuts were applied: **a)** no cuts; **b)** $2m_c \leq m_{c\overline{c}} \leq 2m_D$; **c)** $2m_c \leq m_{c\overline{c}} \leq 2m_D$ and $20^\circ \leq \theta_c \leq 160^\circ$; **d)** $2m_c \leq m_{c\overline{c}} \leq 2m_D$, $p_T^2 \geq 1\,\text{GeV}$, $0.3 \leq z \leq 0.9$ and $60\,\text{GeV} \leq W_{\gamma p} \leq 180\,\text{GeV}$. The p_T^2 and z cut were however not applied to the p_T^2 and z distributions respectively. The positions of the cuts are indicated by the dotted lines. 33

4.5 Pointlike component of the ep cross sections in the color evaporation model as a function of p_T^2, $W_{\gamma p}$ and z calculated in leading order by RAPGAP (shaded) and in next to leading order by the FMNR program (solid line). Both distributions represent the color evaporation model. A cut on the invariant mass of $2m_c \leq m_{c\bar{c}} \leq 2m_D$ was made. For details see text. 35

4.6 Comparison of the γp cross section for photoproduction for fixed target experiments of the published color evaporation model prediction (line) and the color evaporation model cross sections calculated by the FMNR program (black points). $MRS(A')$ was used as PDF. W_γ is the photon energy. 36

4.7 γp cross sections as a function of z, a) as published in [Ha6] and b) as calculated with the FMNR program. For b) the correction factor $Q_0 = 2m_c$ was chosen. A factor of 7 was applied to b). A cut of $p_T^2 \geq 1\,\mathrm{GeV}$ is made for both figures. . . 37

4.8 ep cross sections of the pointlike component of the color singlet model Monte-Carlo generator EPJPSI (dotted line) compared with the cross sections of the FMNR program. The solid line represents the cross section for the FMNR program without the correction factor and the dashed line with the correction factor as described in equation 2.27. The cuts are described in table 4.2. The distributions of the FMNR program were multiplied by a factor 9 to match them to EPJPSI. 39

4.9 γp cross sections as a function of $log(x)$ with arbitrary normalization. The dotted line is calculated from equation 2.14 with the simplified gluon density of equation 2.17 and the solid line is calculated with the gluon density from the PDF set $MRS(A')$. The shaded area is the EPJPSI cross section. The dashed line shows the color evaporation model predictions calculated with the FMNR program with the factor for double counting. 41

4.10 Differential ep cross sections as a functions of a) p_T^2, b) $W_{\gamma p}$ and c) z for the color evaporation model predictions with (dotted line) and without (solid line) double counting factor applied. The dots are data from [Kru00]. $MRS(A')$ was used as proton PDF and the factors $\rho_{J/\Psi} = 0.43$ and $\frac{1}{9}$ were applied to normalize the FMNR distributions to the color evaporation model. The cuts are indicated in the figure, they are applied to the FMNR distributions and the data. The cuts $p_T^2 \geq 1\,\mathrm{GeV}^2$ and $0.3 \leq z \leq 0.9$ are not applied to the p_T^2 and z distribution respectively. The cuts are indicated by the dashed lines. A factor of 9 was applied to all distributions of the FMNR program. 42

4.11 p_T^2 distributions for four different z bins. The distributions are normalized to 1. The normalization factors N for data and EPJPSI are listed in table 4.5. The cuts applied to the four distributions are described in the text. 45

4.12 p_T^2 distributions for four different z bins. The distributions are normalized to 1. The normalization factors are listed in table 4.5. The cuts applied to the four distributions are described in the text. 46

List of Tables

3.1 Classes of diagrams being evaluated for Born and NLO contributions in powers of α_{em} and α_s. 24

4.1 Pointlike and hadronic component of the $c\overline{c}$ pair production cross section for γp and ep collision with various settings in comparison with the data published in [FMNR6, FMNR7]. 27

4.2 Cuts applied to the distributions in figures 4.8. In addition a cut of $Q^2 \leq 1\,\text{GeV}$ was applied. 38

4.3 Cuts and settings applied to the distributions in figures 4.9. 40

4.4 Cuts applied to the FMNR distributions in figures 4.10. In addition a cut of $Q^2 \leq 1\,\text{GeV}$ was applied. 41

4.5 Normalization factors for the double differential distributions of FMNR,EPJPSI and the data. The factor of 9 that was applied to the FMNR program in previous sections was not applied here. 44

A.1 Steering parameters for EPJPSI. Values not listed are set to the default value. A description for each variable is found in the right column. For more details see [Jun1]. 57

A.2 Steering parameters for RAPGAP. Values not listed are set to the default values. A description for each variable is found in the right column. For more details see [Jun2]. 58

A.3 Steering card for the pointlike component of FMNR for electron proton collision with a center of mass energy of 300 GeV and a charm mass of 1.4 GeV. The energy given is half the center of mass energy. The PDF set for the proton is as given in the publication [PDF]. 59

A.4 Steering card for the hadronic component of FMNR for photon proton collision with a center of mass energy of 64.778 GeV and a charm mass of 1.4 GeV. The PDF sets are defined by Frixione et al. and are included in the FMNR program. 71 is the $MRS(A')$ proton PDF and 43 is the $GRV-HO$ photon PDF. 60

A.5 The center of the $W_{\gamma p}$-bins for the 10 GeV $W_{\gamma p}$-bins between 60 GeV and 260 GeV used. 60

A.6 Scale factors used in this analysis. 60

Bibliography

[Aub] J. J. Aubert et al., Phys. Rev. Lett. **33** (1974) 1404

[Aug] J. E. Augustin et al., Phys. Rev. Lett. **33** (1974) 1406

[Bam] A. Bamberger et al., Nucl. Phys **314** (1978) 1 and many others, for a complete list see [Ha3] reference (20) and (21)

[BaR] R. Baier and R. Rückl, Phys. Lett. **B102** (1981) 364; Nucl. Phys. **B201** (1982) 1; Zeit. f. Phys. **C19** (1983) 251

[BBL] G. T. Bodwin, E. Braaten and G. P. Lepage, Phys. Rev. **D46** (1992) 1914

[BBL1] G. T. Bodwin, E. Braaten and G. P. Lepage, Phys. Rev. **D51** (1995) 1125

[BeJ] E. L. Berger and D. Jones, Phys. Rev. **D23** (1981) 1521

[BrC] E. Braaten, Y. Chen, Phys Rev. **D54** (1996) 3216

[Bu1] W. Buchmüller, Phys. Lett. **B353** (1995) 335; W. Buchmüller and A. Hebecker, Phys. Lett. **B355** (1995) 573

[CDF1] CDF Collaboration, F. Abe, et al. preprint **FERMILAB-CONF-95/128-E**, preprint **FERMILAB-CONF-95/136-E**, preprint **FERMILAB-CONF-95/263-E**

[Cha] C.-H. Chang, Nucl. Phys. **B172** (1980) 425

[DuO] D. W. Duke, J. F. Owens, Phys. Lett. **B96** (1980) 184

[Ed1] A. Edin, G. Ingelman and J.Rathsman, Phys. Rev. **D56** (1997) 7317

[EMC1] European Muon Collaboration, J. Aslaman et al., Zeit. f. Phys. **C56** (1992) 21

[Fle] S. Fleming, Int. J. Mod. Phys. **A12** (1997) 3995

[Far] G. R. Farrar, Nucl. Phys **B77** (1974) 429; J. F. Gunion, Phys. Rev. **D10** (1974) 242

[FMNR] private communication from S. Frixione and M. L. Mangano

[FMNR1] S. Frixione, M. L. Mangano, P. Nason, G. Ridolfi, Nucl. Phys. **B373** (1992) 295

[FMNR2] S. Frixione, M. L. Mangano, P. Nason, G. Ridolfi, Phys. Lett. **B319** (1993) 339

[FMNR3] S. Frixione, M. L. Mangano, P. Nason, G. Ridolfi, Phys. Lett. **B308** (1993) 137

[FMNR4] S. Frixione, M. L. Mangano, P. Nason, G. Ridolfi, Nucl.Phys. **B412** (1994) 225

[FMNR5] S. Frixione, M. L. Mangano, P. Nason, G. Ridolfi, Nucl. Phys. **B412** (1994) 225

[FMNR6] S. Frixione, M. L. Mangano, P. Nason, G. Ridolfi, Phys. Lett. **B348** (1995) 633

[FMNR7] S. Frixione, M. L. Mangano, P. Nason, G. Ridolfi, Nucl. Phys. **B454** (1995) 3

[FMNR8] S. Frixione, M. L. Mangano, P. Nason, G. Ridolfi, Nucl. Phys. **B483** (1997) 321

[FMNR9] S. Frixione, M. L. Mangano, P. Nason, G. Ridolfi, **hep-ph9702287 v2** (1997), published in Heavy Flavours ed. by A.J. Buras and M. Lindner, World Scientific (1992) 785

[FMNR10] S. Frixione, M. L. Mangano, P. Nason, G. Ridolfi, notes to the program found in /h1/h1gen/fmnrdoc.txt

[Fr1] H. Fritsch, Phys. Lett. **B67** (1977) 217

[H1] H1 Collaboration, I. Abt. et al., Nucl. Instr. and Meth. **A386** (1997) 310 and Nucl. Instr. and Meth. **A386** (1997) 348

[H1Z] H1 Collaboration, Nucl. Phys. **B 472** 3 (1996); ZEUS Collaboration, Z. Phys. **C 76** (1997) 599

[Ha1] F. Halzen, Phys. Lett. **B69** (1977) 105; F. Halzen and S. Matsuda, Phys. Rev. **D17** (1978) 1344

[Ha2] J. F. Amundson, O. J. P. Eboli, E. M. Gregores and F. Halzen, Phys. Lett. **B372** (1996) 127

[Ha3] O. J. P. Eboli, E. M. Gregores and F. Halzen, **MADPH-96-965**, (1996)

[Ha4] J. F. Amundson, O. J. P. Eboli, E. M. Gregores and F. Halzen, Phys. Lett. **B390** (1997) 323

[Ha5] O. J. P. Eboli, E. M. Gregores and F. Halzen, Nucl. Phys. Proc. Suppl. **71** (1999) 349

[Ha6] O. J. P. Eboli, E. M. Gregores and F. Halzen, Phys. Lett. **B451** (1999) 241-246

[Ha7] J. F. Amundson, O. J. P. Eboli, E. M. Gregores and F. Halzen, Phys. Rev. **D60** (1999) 117501

[Ha8] O. J. P. Eboli, E. M. Gregores and F. Halzen, Phys. Rev. **D61** (2000) 34003

[Jun1] H. Jung, **http://www-h1.desy.de/ jung/epjpsi.html** (1998); Eds. W. Buchmüller, G. Ingelman, Proceedings 'Physics at HERA' **Vol. 3** (1991) 1488

[Jun2] H. Jung, **http://www-h1.desy.de/ jung/rapgap.html** (1999); H. Jung, Comp. Phys. Comm. **86** (1995) 147 (1999)

[Kra] M. Krämer, Int. J. Mod. Phys. **A12** (1997) 3985

[Kra1] M. Krämer, Proceedings of the Ringberg Workshop “New Trends in HERA Physics”, Germany (1997); **hep-ph/9707449**

[KrB] M.Beneke, M. Krämer, Phys Rev. **D55** (1997) 5269

[Kru] K. Krüger, **http://www-h1.desy.de/publications/theses_list.html**

[Kru00] K. Krüger, PhD thesis soon to be published and private communication

[Mey] A. Meyer, **DESY-Thesis-1998-012** (1998) 56

[Miz] J. K. Mizukoshi, **SLAC-PUB-8296** (1999)

[NDE] P. Nason, S. Dawson, R. K. Ellis, Nucl. Phys. **B303** (1988) 607

[PDF] H.Plothow-Besch, **CERN-PPE 1997.04.07**

[Rot] I. Rothstein, **hep-ph/9911276 v2** (1999), Submitted to Phys. Lett. **B**

[Sjo] T. Sjöstrand, Phys. Comm. **39** (1986) 347, Phys. Comm. **43** (1987) 367, Phys. Comm. **82** (1994) 74

[WW] C. F. Weiszäcker, Z. Phys **88** (1934) 612; E. J. Williams, Phys. Rev. **45** (1934) 729

Acknowledgments

Most of all I want to thank Prof. Dr. B. Naroska for the interesting and challenging topic and the always helpful advices and a very good and supportive supervision during the past year. I want to thank Prof. Dr. V. Blobel for being the second expert evaluating this thesis.
I also want to thank everybody that helped me with this thesis and the correction of it. Special thanks go to Dirk, Andreas and Carsten for endless time spent reading my thesis and a flood of good advices, Katja for being always helpful and providing me with the data points used in this analysis, Susanne for introducing me to the programs and procedure used at H1. Tim has to be thanked for hours of support whenever my computer decided to bug me and I didn't know a way out anymore. Of course the group around Beate Naroska was most helpful and sustained me with lots of help and long coffee breaks (although lunchtime was a bit early).
Special thanks go to Christoph Grab, Stefano Frixione, Michelangelo Mangano, Eduardo Gregores and Hannes Jung for their helpful advice and information.
I want to thank Chia Fung for reading this thesis and keeping me sane and happy even when I worked all night long. I also want to thank Ede for distracting for an hour or two for many evenings. And last but not least I want to thank my parents, grandparents and Eva for all their support.